Sphingolipids with Very Long-chain Fatty Acids Regulate Vacuole Fusion During Tethering and Docking

Logan R. Hurst[1], Chi Zhang[1], Thomas D.D. Kazmirchuk[2], David A. Rivera-Kohr[1], Christopher L. Brett[2], and Rutilio A. Fratti[1,3,4]

1. Department of Biochemistry, and University of Illinois Urbana-Champaign, Urbana, IL, USA

2. Department of Biology, Concordia University, Montreal, QC, Canada

3. Center for Biophysics and Quantitative Biology, University of Illinois Urbana-Champaign, Urbana, IL, USA

4. Address correspondence to: Rutilio A. Fratti (rfratti@illinois.edu)

ORCID
Rutilio Fratti **-** https://orcid.org/0000-0001-9109-6666

Running title: Elo3p regulation of vacuole fusion via lipid rafts

Keywords: Membrane fusion, SNARE, Rho1p, lipid raft, Vac8p, Elo3p

Abbreviations used: VLCFA, Very long-chain fatty acid; LCB, long-chain base; FAS, fatty acid synthase; PtdInsP, phosphatidylinositol phosphate; IPC, inositolphosphoryl ceramide.

Summary

Many sphingolipids contain very-long chain fatty-acids with 26 carbons. The deletion of Elo3, the elongase that adds the final two carbons results in pleiotropic effects that negatively alter membrane fusion at the tethering and docking stages.

Abstract

The role of sphingolipids in controlling the endolysosomal membrane trafficking remains unclear. Here, we show that in *Saccharomyces cerevisiae* sphingolipids containing very long-chain fatty-acids (VLCAs) promote homotypic vacuolar fusion. Yeast that lack the C26 VLCA elongase Elo3p display morphological and vacuolar abnormalities. Vacuoles isolated from these cells displayed reduced levels of *in vitro* fusion, which we traced to a block in tethering and docking. We found that C26 VLCFA deficient yeast mislocalize fusion markers, and the small GTPases Rho1p and Ypt7p fail to selectively concentrate at the boundary and vertex domains of vacuoles isolated from these yeasts. Surprisingly, we only observed mild changes to the localization of other regulatory lipids, but membrane fluidity and solubility was significantly altered. Taken together, these results suggest that sphingolipids containing C26 VLCFAs act as regulatory lipids in the homotypic vacuolar fusion cascade by assembling membrane microdomains that promote the protein and lipid machinery required for the tethering and docking of vacuoles.

Introduction

The lipid composition of a cell is extremely diverse and complex, and the physical properties of different biological membranes are dictated by this composition (Harayama and Riezman, 2018). The finely tuned lipid composition of organelle and vesicle membranes is a key determinant in the ability of a cell to carry out trafficking events such as exocytosis and organelle fusion, and changes to the membrane can drastically affect these essential processes (Johansen et al., 2012; Starr and Fratti, 2019).

Membrane fusion is carried out in four experimentally determined steps (Priming, Tethering, Docking, and Fusion), which are conserved throughout secretion, autophagy, and homotypic vacuolar fusion (Conradt et al., 1994; Wickner and Schekman, 2008; Wickner, 2010). In the case of *Saccharomyces cerevisiae*, the spatiotemporal localization and activity of many proteins and lipids that participate in homotypic vacuole fusion are well understood. Priming of the membranes is dependent on the conversion of phosphatidic acid (PA) to diacylglycerol (DAG) by Pah1p in the membrane, and the action of the chaperone proteins Sec17p (α-SNAP) and the AAA+ ATPase Sec18p (NSF), which releases SNAREs (soluble NSF attachment protein receptors) (Vam3p, Nyv1p, Vti1p, and Vam7p) from inactive cis-bundles (Mayer et al., 1996; Mayer and Wickner, 1997; Starr et al., 2016). This is followed by tethering of the vacuoles through interactions between a Rab GTPase (Ypt7p), and the heterohexameric HOPS (homotypic fusion and protein sorting) complex (Miner et al., 2016; Seals et al., 2000; Stroupe et al., 2006). Docking of the vacuoles can be visualized with

fluorescent microscopy, where they form large, flat regions after they become tightly apposed, which is facilitated by SNARE proteins from opposite membranes bundling together in a tight, coiled-coil motif (trans-SNARE bundle) (Collins and Wickner, 2007; Wang et al., 2002). Fusion is completed after hemifusion between the cytoplasmic outer leaflets leading to pore formation between the two organelles, finally followed by full content mixing between the two organelles (Jun and Wickner, 2007; Mattie et al., 2017). Tethering, docking, and fusion steps also require the activity of the Rho-family GTPases Cdc42p and Rho1p, which control cycles of actin remodeling at the vacuole membrane (Eitzen et al., 2002; Isgandarova et al., 2007; Logan et al., 2010). Studies have shown a requirement for small amounts of regulatory lipids, which are enzymatically modified at specific times throughout the endosomal maturation and homotypic vacuole fusion processes (Starr and Fratti, 2019). In some cases, these regulatory lipids have been found to co-localize with fusion machinery proteins in a region termed the “vertex domain”, the ring-like area surrounding two membranes in contact during the docking stage (Fratti et al., 2004; Wang et al., 2002). The regulatory glycerophospholipids diacylglycerol (DAG), phosphatidic acid (PA) and a number of phosphatidylinositol phosphates (PtdInsP) have been shown to influence the recruitment and activity of Rab and Rho GTPases, chaperone proteins, HOPS, SNAREs, and actin (Karunakaran et al., 2012; Karunakaran and Fratti, 2013; Miner et al., 2016; Miner et al., 2017; Miner et al., 2019; Starr et al., 2016).

In contrast to glycerophospholipids, there are only a few studies that investigate the role of sphingolipids in the system of homotypic vacuole fusion. In wild type yeast very-long-chain fatty acids (VLCFAs) are almost exclusively found bound to long chain bases (LCBs) to form a ceramide or glycosphingolipid, as free VLCFAs in cell extracts are barely detectable (Lester et al., 1993). Baker’s yeast is known to contain three fatty acid elongases (Elo1p, Elo2p, and Elo3p), which catalyze the condensation of a malonyl-CoA unit with a long-chain fatty acyl-CoA within the endoplasmic reticulum (ER) membrane. Each of these enzymes has an inherent substrate specificity and unique VLCFA major product, such as Elo3p displaying specificity for long- to very-long-chain fatty acid substrates, and producing VLCFAs up to 26-carbons in length (Denic and Weissman, 2007; Rössler et al., 2003). The C26 VLCFA is likely critical for the function of yeast sphingolipids in membranes based on research demonstrating that this particular species of fatty acid is found in the vast majority sphingolipid species in wild-type yeast (Ejsing et al., 2009). Studies with yeast lacking functional elongase enzymes have uncovered links between sphingolipids and Vps21p-related endosomal maturation, vacuolar acidification, and vacuolar morphology/function, but their role as regulatory lipids in membrane fusion remains unclear (Chung et al., 2003; Faergeman et al., 2004; Gaigg et al., 2001; Kohlwein et al., 2001; Obara et al., 2013).

The Rab subfamily of small GTPases has long been known as regulators of membrane trafficking, and Ypt7p function has been well established at the vacuole (Wichmann et al., 1992) (Haas et al., 1995) (Vollmer et al., 1999) (Eitzen et al., 2000; Karim et al., 2018; Lachmann et al., 2012; Langemeyer et al., 2018; Price et al., 2000). Additionally, the Rho subfamily’s contributions to the fusion cascade at the yeast

vacuole have been investigated, which showed they regulate actin polymerization at multiple sites within a cell (Eitzen et al., 2001; Eitzen et al., 2002; Isgandarova et al., 2007; Jones et al., 2010; Logan et al., 2010; Logan et al., 2011). While many members of the Rab- and Rho-subfamilies of small GTPases associate with membranes via the post-translational attachment of a C-terminal prenyl-anchor(s), specific sub-cellular localization has been shown to be dependent on C-terminal polybasic regions (PBRs), protein myristoylation/palmitoylation, GTPase-effector interactions, and biophysical properties of the membrane, e.g. headgroup charge, fatty acid unsaturation, lipid packing etc. (Abe et al., 2003; Kulakowski et al., 2018; Michaelson et al., 2001; Ohya et al., 1993; Pechlivanis and Kuhlmann, 2006; Wu and Brennwald, 2010).

Both isolated membranes and organelles purified from live yeast cells have been found to form lipid rafts, also known as membrane microdomains and/or nanodomains. These are transient, sub-organellar domains, which phase separate within a membrane based on differences in lipid and protein composition, which alter the membrane's fluidity. These domains are highly enriched in sterols, sphingolipids and other lipids with saturated acyl chains, and display liquid-ordered-like properties (Klose et al., 2010; Sezgin et al., 2017; Toulmay and Prinz, 2013). Recently, it was shown that isolated yeast vacuoles do indeed contain regions of the vacuolar membrane with ergosterol-rich domains that are also enriched in the regulatory lipids PtdIns 3-phosphate (PtdIns(3)P), PtdIns 3,5-bisphosphate (PtdIns(3,5)P_2), and PtdIns 4-phosphate (PtdIns(4)P) (Takatori et al., 2016; Tomioku et al., 2018). In the work below we present evidence that a lack of C26-containing VLCFAs leads to a disruption in the stable formation of vertex regions of docked lysosome-like vacuoles. Upon deletion of the only C26 VLCFA biosynthetic gene (*ELO3*) we observe a decrease in the measurable amounts of homotypic vacuolar fusion and morphological changes to the vacuole. We show that this decrease in fusion is largely due to the mislocalization of fusion machinery proteins; including Rab- and Rho-family GTPases, leading to subsequent defects in the tethering and docking steps of vacuole fusion. We show that fusion proteins from mutant cells are solubilized from the vacuolar membrane in a manner similar to wild-type vacuoles that have been treated with mild detergents. Evidence suggests that a lack of C26 VLCFAs prevents the specific clustering and enrichment of fusion proteins at the vertex ring between apposed vacuoles, likely due to a disruption of the membrane microdomains that are enriched for fusion proteins.

Results

Yeast without Elo3p have misshapen vacuoles and are deficient in lipid mixing and content mixing. To probe the role that C26 VLCFA-containing sphingolipids play in vacuole fusion the *ELO3* gene (formerly *SUR4*) was deleted from *S. cerevisiae* (Materials and Methods), and vacuole morphology was probed in live cells. Wild type BJ3505 yeast grown to log phase in YPD are round, contain vacuoles that occupy roughly half of the cell volume, and most cells have one or two vacuoles as visualized by fluorescent microscopy with the lipophilic dye FM4-64 **(Fig. 1)**. However, BJ3505 *elo3*Δ cells are much larger, misshapen,

and often have multiple vacuoles **(Fig. 1A)**. Previous studies have described the shape of *ELO3* mutants as "dumbbell-shaped" (Desfarges et al., 1993), and we observed similar elongated and clustered cells. The knockout cells frequently had large, misshapen vacuoles, with many small, clustered vacuoles, which corresponds to Class F vacuole morphology (Raymond et al., 1992). We quantified these observations by counting the number of vacuoles in each cell, which confirmed that *elo3*Δ cells have multiple fragmented vacuoles **(Fig. 1B)**. We then calculated the area each vacuole occupied in microscopic images and found that *elo3*Δ vacuoles vary widely in size **(Fig. 1C)**. We next visualized live yeast after treatment with known inhibitors of *de novo* sphingolipid biosynthesis **(Fig. 1)**. Myriocin blocks the rate-limiting step of LCB synthesis by serine-palmitoyl transferase complex (Lcb1p/Lcb2p) (Kvam et al., 2005; Nagiec et al., 1994), Aureobasidin A blocks inositolphosphorylceramide (IPC) synthesis by Aur1 (Hashida-Okado et al., 1996; Voynova et al., 2015), and cerulenin has been reported to inhibit both the soluble fatty acid synthase (FAS) complex and the microsomal VLFCA elongase system at high concentrations (Kvam et al., 2005). While all three inhibitors perturbed cell and vacuole morphology, treatment with Aureobasisdin A and cerulenin reliably produced a similar phenotype to that of an Elo3p deletion (abnormal cell shape and Class F vacuole morphology), while treatment with myriocin caused a severe fragmentation phenotype (Class B vacuole morphology) and a smaller cell size **(Fig. 1A-C)**. This is intriguing as IPC has been shown to be enriched at the yeast vacuole (Hechtberger et al., 1994), and has been suggested (along with ceramide) to be required for proper vacuole morphology and function (Faergeman et al., 2004). Yeast strains that are impaired in vacuolar fusion have been shown to have an increased sensitivity to the presence of caffeine and sorbitol in the growth medium (Tedrick et al., 2004). We found that *elo3Δ* yeast exhibit a severe sensitivity under both conditions **(Fig. 1D)**. These results strongly suggest that C26 VLCFA's are necessary for proper vacuole morphology and function in yeast.

To examine how the lack of functional Elo3p affects homotypic fusion, vacuoles were isolated from wild-type and *elo3*Δ strains in BJ3505 and DKY6281 backgrounds via density floatation gradient as previously described (Conradt et al., 1992; Haas et al., 1994). Isolated vacuoles were incubated under standard fusion conditions, and *in vitro* fusion was monitored with proPho8p maturation upon content mixing. Using this assay, we found that *elo3*Δ vacuole fusion was only about 60% as efficient relative to wild type vacuoles **(Fig. 2A)**. To visualize the rate of fusion of *elo3*Δ vacuoles the data was plotted normalized to its own fusion max after 60 min. This shows that rate of fusion is slightly reduced during the first 20-30 min when vacuoles came from *elo3*Δ cells **(Fig. 2A, open red circles)**. The measured decrease of fusion at this time in the reaction is indicative of a defect in the tethering step of the cascade. We next probed the severity of the fusion defect by mixing fusion partners from different genetic backgrounds. Fusion reactions between vacuoles that were isolated solely from the *elo3*Δ background showed a severe reduction in fusion relative to wild type **(Fig. 2B, lane 5)**. However, when fusion partners were mixed from wild type and *elo3*Δ backgrounds the fusion defect was partially rescued **(Fig. 2B, lanes 3 & 4)**. This data suggests sphingolipids

containing C26 VLCFAs positively regulate homotypic vacuolar fusion, possibly at the tethering or docking step due decreased *in vitro* fusion at early time points.

To determine a possible contribution VLCFAs make to hemifusion, the step directly following docking, vacuoles isolated from BJ3505 wild-type and BJ3505 *elo3*Δ cells were used in lipid mixing experiments. After labeling vacuoles with rhodamine B-conjugated phosphatidylethanolamine (Rh-PE) in self-quenching concentrations (Reese et al., 2005; Reese and Mayer, 2005), the increase in fluorescence via dequenching from outer leaflet mixing was monitored. Using this method, we found that vacuoles isolated from *elo3*Δ cells displayed significantly reduced amounts of fluorescence **(Fig. 2C)**. These results reinforce the observation that vacuoles from *elo3*Δ are defective in the tethering/docking stages of fusion and are not able to reach significant levels hemifusion/content mixing. The VLCFAs present in sphingolipids have been suggested to help stabilize highly curved membranes through their ability to modulate membrane dynamics and fill voids that form between the inner and outer leaflets of bilayers (Molino et al., 2014). Surprisingly, we detected no difference in the relative amount of lipid mixing to content mixing between wild type and *elo3*Δ **(Fig. 2D)**, and also no major time delay between lipid mixing and content mixing **(Fig. 2E)**, indicative of normal pore formation kinetics (Karim et al., 2018). Together, these results show C26 VLCFAs positively regulate homotypic vacuole fusion, evidenced by morphological changes in live cells, and a significant reduction in the measurable *in vitro* lipid- and content mixing of isolated vacuoles. The observed block at early points in the fusion reaction that don't seem to affect the kinetics of pore formation suggest Elo3p regulates an upstream step of the cascade.

The tethering and docking steps are blocked in *elo3Δ* vacuole fusion due to the loss of small GTPases from the vertex domain.

We rationalized that the observed reductions to *in vitro* hemifusion and content mixing of vacuoles isolated from *elo3*Δ yeast could be due to a mislocalization of fusion machinery proteins, possibly due to alterations in anterograde trafficking or secretory pathways. To this end, the levels of fusion proteins normally associated with isolated vacuoles were probed via immunoblotting. Similar to a previous report (Faergeman et al., 2004) there was a significant decrease in the amount of membrane-embedded SNAREs (Vti1p/Nyv1p/Ykt6p) associated with vacuoles isolated from yeast lacking Elo3p, and we also found significant decreases to chaperones (Sec17p/Sec18p), small GTPases (Rho1p/Ypt7p/Vps21p), and the HOPS subunit Vps33p **(Fig. 3A)**. Surprisingly, we found the integral vacuolar ATPase subunit Vph1p was slightly decreased, which was not found to be the case in a previous study (Chung et al., 2003). Unexpectedly, we also observed a marked decrease in vacuole-associated actin, as this protein is often used as a loading control in our system. We attempted to circumvent this by using Pgk1p as a loading control, however vacuoles from *elo3*Δ yeast also displayed a reduction in this protein. In contrast to their vacuolar distribution, the relative levels of these vacuole fusion proteins are consistently similar, if not slightly increased in the *elo3*Δ background when total protein from whole-cell extracts were analyzed **(Fig. 3A)**. This data suggests

that the intracellular trafficking of many vacuolar fusion proteins is strongly influenced by the production of C26 VLCFAs, especially those that bypass the endosome via the AP-3 pathway (Klionsky and Emr, 1989) (Feyder et al., 2015). The decrease in mature Pho8p (mPho8p) signal could plausibly be the reason for decreased signal in the content mixing assay **(Fig. 2A)**, however this would not account for the significant decrease in lipid mixing **(Fig. 2C)**.

We were intrigued by the noticeable loss of the V-ATPase subunit Vph1p on isolated vacuoles **(Fig. 3A)**. The vacuole fusion reaction is inhibited when the proton gradient between the vacuole lumen and cytosol is abrogated, and sphingolipids have previously been identified as necessary components for a functional V-ATPase complex (Chung et al., 2003; Peters et al., 2001). To test if vacuoles isolated from *elo3*Δ yeast are capable of acidification we utilized an acridine orange fluorescence quenching assay (Müller et al., 2002). After the addition of ATP to the reaction, the fluorescence signal of the acridine orange decreases as protons enter the lumen. Using this assay, we found that vacuoles isolated from the *elo3*Δ strain have significantly impaired proton-pumping ability compared to the wild-type vacuoles **(Fig. 3B)**. The vacuole stores large amounts of Ca^{2+} within the lumen, which has been shown to efflux into the cytosol following trans-SNARE pairing at the docking step of fusion (Merz and Wickner, 2004). To confirm that *elo3*Δ vacuoles are defective for trans-SNARE pairing we monitored calcium efflux during the course of a fusion reaction. We found that *elo3*Δ vacuoles are unable to release luminal calcium stores to the same extent as vacuoles isolated from WT yeast **(Fig. 3C)**. Together these results strengthen the argument for regulation of tethering and docking of yeast vacuoles by sphingolipids with C26 VLCFAs.

We wanted to ensure that the observed decrease to *in vitro* content mixing was due to an inhibition of one of the fusion steps, and not perturbed trafficking and maturation of proPho8p. To do this we monitored the docking step of purified vacuoles using fluorescent microscopy as previously described (Eitzen et al., 2002; Fratti et al., 2004; Wang et al., 2002). Vacuoles isolated from each strain were incubated for 20 min to allow for tethering and docking to occur, and then visualized **(Fig. 4A)**. Each condition was scored for docking by counting the number of vacuoles per docked cluster **(Fig. 4B)**. Wild-type vacuoles clustered very well, with a majority of the tethered/docked clusters containing five or more vacuoles. To specifically inhibit the tethering step, we incubated wild-type vacuoles under the same conditions in the presence of presence of purified recombinant Gdi1p, a guanine-nucleotide dissociation inhibitor (GDI) that functions in Rab-GTPase turnover. In these reactions the GDI protein binds to GDP-bound Rab proteins and sequesters their activation by preventing GTP binding and subsequent tethering action (Starai et al., 2007). The addition of rGDI to docking reactions caused a strong shift from multiple vacuoles per cluster to only one or two. Finally, we incubated vacuoles isolated from *elo3*Δ yeast under normal docking conditions and found that they were impaired in this step, similar to wild-type vacuoles inhibited by GDI treatment **(Fig. 4B)**. These experiments confirmed that C26 VLCFAs are necessary for proper tethering and docking necessary for the fusion of purified vacuoles.

The significant loss of small GTPases Ypt7p and Rho1p from vacuolar membranes **(Fig. 3A)** is intriguing, as these proteins are known to function in the tethering and docking steps of homotypic fusion (Eitzen et al., 2000; Eitzen et al., 2001; Eitzen et al., 2002; Haas et al., 1995; Isgandarova et al., 2007; Jones et al., 2010; Karim et al., 2018; Lachmann et al., 2012; Langemeyer et al., 2018; Logan et al., 2010; Logan et al., 2011; Ohya et al., 1993; Price et al., 2000; Vollmer et al., 1999; Wichmann et al., 1992). N-terminal fusion proteins of GFP-Ypt7p under control of the native promoter (Wang et al., 2002), and constitutively expressed DsRed-Rho1p on a centromeric plasmid (this study) were expressed in live yeast. We monitored the localization of GFP tagged Ypt7p in wild-type and *elo3*Δ yeast. Wild-type cells had strong GFP signal at the vacuolar membrane, which was enriched at puncta between membranes that represent the vertex domains of docked vacuoles **(Fig. 5A)**. The *elo3*Δ cells again showed significant vacuolar fragmentation compared to wild-type, and the GFP fluorescent signal appeared weaker on these vacuoles. Although there is a significant increase in the number of small vacuoles per cell **(Fig. 1B)**, the puncta we observed were often not enriched at the vertex of docked vacuoles in *elo3*Δ cells, and GFP signal had poor co-localization with FM4-64 signal **(Fig. 5A)**. The observed decrease of Ypt7p on purified vacuoles, vertex domains in live yeast, and the decreased fusion at early time points indicated a defect in the tethering and docking steps of fusion in *elo3*Δ yeast. These experiments suggest that C26 VLCFAs may be necessary for vertex enrichment of fusion proteins on vacuoles. Previous studies demonstrated that the GFP-Ypt7p construct is enriched at the vertices of docked vacuoles, and this enrichment is dependent on the presence of regulatory PtdIns(4,5)P_2 (Fratti et al., 2004; Wang et al., 2002). We therefore purified vacuoles from yeast that expressed the fluorescent GTPase proteins and monitored localization during docking experiments. We also observed very sharp vertex localization of GFP-Ypt7p when the vacuoles were isolated from wild-type cells and visualized in docking reaction **(Fig. 5B)**. When the vacuoles were isolated from the *elo3*Δ strain, we observed multiple vertex puncta, however there was notably diffuse GFP signal outside of the vertex regions into the boundary and outer regions **(Fig. 5B)**. We measured the distribution of GFP-Ypt7p and FM4-64 signal of docked vacuoles, which confirmed GFP signal was not enriched at the vertex of docked vacuoles in *elo3*Δ cells **(Fig. 5A and 5B)**.

Wild-type yeast expressing the Rho1p chimera showed mostly plasma membrane and vacuole membrane localization, with some dense patches of fluorescence near the area of cytokinesis and in the area of the boundary and vertex regions of docked vacuoles **(Fig. 5C)** (Yoshida et al., 2009). In the *elo3*Δ cells the membrane localization of the fluorescent Rho1p is dispersed and is frequently absent from region of cytokinesis. We also observed fluorescent signal in the vacuolar lumen in many *elo3*Δ cells, indicating Rho1p may be targeted for degradation when it is incorrectly solubilized from vacuole membranes **(Fig. 5C)**. We visualized these differences in localization using line scan analyses and found that DsRed signal closely followed the signal of vacuole membrane marker MDY64 in the wild-type membranes, but this fluorescence co-localization is again perturbed in the *elo3*Δ cells **(Fig. 5C)**. To our knowledge Rho1p has not been

visualized on purified vacuoles to date. Here we show that DsRed-Rho1p was present on purified wild-type vacuoles, and that it localized strongly to the boundary regions of apposed vacuoles during the course of a docking reaction **(Fig. 5D)** (Fratti et al., 2004; Wang et al., 2002). The dsRed-Rho1p fluorescence was also found on vacuoles isolated from the *elo3*Δ strain, but the signal associated with the boundary was significantly decreased. These results suggest that the specific localization of small GTPases that regulate vacuolar fusion was strongly influenced by the cell's ability to produce C26 VLCFAs.

Actin localization, but not polymerization rate, at the vacuole is reduced in *elo3*Δ cells.

The Rho-family of small GTPases are necessary to activate actin remodeling at the plasma membrane for secretion and division processes (reviewed in (Jaffe and Hall, 2005), and at the vacuole for homotypic vacuolar fusion (Eitzen et al., 2002; Isgandarova et al., 2007; Karunakaran et al., 2012). It seemed that the observed reduction of membrane associated Rho1 on the vacuolar membrane could be a cause for the reduction in actin localization at the vacuole, and possibly actin remodeling, which is necessary for efficient fusion. Previous studies have shown that purified yeast actin labeled with a fluorophore localized to the vertex domain of docked vacuoles, and this localization is strongly influenced by PtdIns(4,5)P_2 levels in the membrane (Karunakaran et al., 2012). To attempt to visualize actin associated with the yeast vacuole *in vivo*, we utilized a fluorescent chimera made from the first 17 amino acids of Abp140p fused to two copies of mCherry (Kilchert and Spang, 2011). We were able to use this construct to visualize actin patches that associated with the cell periphery (plasma membrane and/or cortical ER membranes) and vacuole membranes in both cell types, although the *elo3*Δ cells displayed noticeably stronger cytosolic signal **(Fig. 6A, B)**. We next utilized a time course microscopic imaging analysis, which showed that the fluorescent Abp140p construct associated with tethered/docked vacuoles in wild-type cells during a fusion event. The fluorescence signal it was pushed away from the boundary region as it briefly concentrates at the vertices and is ultimately pushed to the outer regions surrounding the vacuole during the fusion process **(Fig. 6B, top panels)**. When *elo3*Δ cells were monitored under the same conditions, there was strong cytosolic mCherry fluorescence as well as a buildup in the boundary region between the tethered/docked vacuoles **(Fig. 6B, bottom panels)**. The buildup of mCherry signal in the boundary region may indicate impaired actin remodeling. These experiments reinforce the observed loss of actin from purified *elo3*Δ vacuoles **(Fig. 3A)**.

Vacuoles isolated from yeast have been shown to stimulate actin polymerization via the Rho-GTPases Cdc42p and Rho1p in an *in vitro* pyrene-actin assay (Isgandarova et al., 2007). We assumed that the decrease in Rho-GTPases, actin, and actin-binding proteins when C26 VLCFAs are absent would result in a significant decrease in actin polymerization activity (APA). Surprisingly, when we performed *in vitro* actin polymerization assays, we were unable to detect a significant decrease in polymerization rates when vacuoles came from cells lacking Elo3p **(Fig. 6C)**. As controls for increasing and decreasing the polymerization rates of actin we included reactions containing jasplakinolide and latrunculin A, respectively. These results

reinforce the idea that the absence of Elo3p activity strongly affects the vacuolar localization of Rho1p and Act1p, but it does not have a significant effect on the rate of *in vitro* Rho-stimulated pyrene-actin polymerization. This data suggests that even though actin is lost from the vacuole membrane, the actin polymerization machinery (Las17p, Arp2/3p, Vrp1p) is still present and functional on vacuoles isolated from *elo3*Δ cells, but this requires further study. Taken together, these results suggest that C26 VLCFAs are necessary for actin localization and remodeling at the vacuole, but not the polymerization step itself.

Other regulatory lipids seem mostly unaffected by the loss of C26 VLCFAs

Rho-family proteins have been shown to have ionic interactions with PtdInsP's via stretches of C-terminal lysine residues that create poly-basic regions (PBRs) very close to the CAAX prenylation sequence (Michaelson et al., 2001; Yoshida et al., 2009), but there are no known physical interactions with sphingolipids to date. There are studies that, taken together, support a possible model for sphingolipid-dependent Rho localization to the vertex domain. It has recently been shown that IMP-deficient, ergosterol- and sphingolipid-rich domains of the yeast vacuole are similarly enriched in PtdIns(3)P, PtdIns(4)P, and PtdIns(3,5)P_2 (Takatori et al., 2016; Tomioku et al., 2018). This raises the possibility that a lack of C26 VLCFAs reduces the tendency for these liquid ordered-like regions to coalesce in live cells. This lack of raft domains may also prevent the localized enrichment of Rho proteins and fusion proteins, many of which are known to have affinity for PtdInsPs in the vertex region of docked vacuoles. To further investigate the possibility that regulatory PtdInsP localization at the vacuole depends on C26 VLCFAs, docking experiments were also performed in the presence of exogenous Cy3-FYVE as previously described (Fratti et al., 2004). This high affinity PtdIns(3)P-binding construct contains two copies of the FYVE domain from mouse Hrs (Gillooly et al., 2000). We were mildly surprised to find practically no difference in the vertex enrichment of Cy3-FYVE bound to PtdIns(3)P **(Fig. 7A)**. This suggests that the vacuole localization of regulatory PtdIns(3)P is mostly unaffected by the loss of C26 VLCFAs from the deletion of *ELO3*.

The formation of membrane lipid rafts or nanodomains in yeast membranes is strongly influenced by the amount of sphingolipids and ergosterol (Klose et al., 2010; Toulmay and Prinz, 2013), and previous studies have shown that ergosterol concentrates at vertex regions during vacuolar fusion and sterol-enriched vacuoles show enhanced fusion (Fratti et al., 2004; Tedrick et al., 2004). We aimed to investigate if the lack of C26 VLCFA-containing sphingolipids would affect the vertex localization of ergosterol. Using sub-inhibitory amounts of the fluorescent macrolide filipin III, which binds to ergosterol, we compared the fluorescence of wild-type and *elo3*Δ docked vacuoles **(Fig. 7B)**. When the docking reactions between wild-type vacuoles were visualized, we observed strong fluorescence as puncta at the vertex and at the boundary domains. When vacuoles isolated from *elo3*Δ cells were incubated with filipin III we observed less fluorescence in general, but the relative levels of vertex enrichment between WT and *elo3*Δ appear identical. These results indicate a slight decrease in the amount of ergosterol in the vacuole, but have similar amounts of sterol vertex enrichment, and no obvious disruption to the membrane microdomains that form at vertex regions.

Altogether, the data suggests that yeast sphingolipids containing C26 VLCFAs don't strongly affect the localization of other regulatory lipids.

Detergent-insoluble membrane composition changes, possibly due to an increase in membrane fluidity, when cells lack C26 VLCFAs

The observation that a lack of VLCFAs disrupts the vertex region of apposed vacuoles raises the possibility that the vertex may be similar in nature to a membrane nanodomain or lipid raft, whose formation is dependent on the presence of sphingolipids and sterols (Anderson and Jacobson, 2002; Bagnat et al., 2000; Brown and Rose, 1992; Drevot et al., 2002; Klose et al., 2010; Peng et al., 2006; Röper et al., 2000; Toulmay and Prinz, 2013). To our knowledge, none of the canonical vacuolar fusion proteins have been probed for nanodomain localization using purified vacuoles to date, but the vacuolar proteins Vac8p, Vph1p, and Pho8p have been localized to microdomain rafts from whole-cell membrane isolations (Bagnat et al., 2000; Peng et al., 2006). Using a similar method, we subjected isolated vacuoles to a 4°C incubation in the presence or absence of detergent, separated the samples on a density gradient, and harvested fractions for SDS-PAGE and Western blotting. In the absence of detergent, soluble proteins such as Pgk1p distribute throughout the gradient while concentrating in the bottom high-density fractions **(Fig. 8A, WT, no detergent, lanes 7-10)**. Membrane embedded (Vph1p, Pho8p), palmitoylated (Vac8p), and prenylated (Ypt7p, Rho1p) proteins tend to float to the upper low-density fractions **(Figure 8A, WT, no detergent, lanes 1-3)**, similar to previous reports (Peng et al., 2006). When *elo3*Δ vacuoles were subjected to the same density gradient, every protein of interest was distributed more evenly throughout the gradient, even without the addition of detergent **(Fig. 8A, *elo3*Δ, no detergent, lanes 6-10)**. This result was indicative of an increase in density of the vacuoles used for isolation, and/or a decrease in the affinity of membrane associated proteins for the vacuolar membrane, enforcing the idea that VLCFAs are necessary for homeostasis of the vacuolar proteome. Initial studies of detergent insoluble membranes first recognized the incomplete solubilization of GPI-linked proteins in the apical membranes of epithelial cells following incubation with the strong non-ionic detergent Triton X-100 (Anderson and Jacobson, 2002). When vacuoles from either the wild-type or *elo3*Δ background were treated with 1% Triton X-100, the distribution of every protein investigated was shifted to the soluble heavy fractions (data not shown), indicating the raft domains formed in the vacuole membrane may be held together by weaker interactions than those seen in the epithelial membrane and yeast plasma membrane, where sphingolipid and ergosterol levels are significantly higher.

Because the strong detergent solubilized all the vacuolar proteins of interest, we employed the use of mild non-ionic detergents Brij98 and Lubrol WX. These detergents have been utilized in studies to isolate biologically relevant rafts from mammalian and yeast membrane systems (Drevot et al., 2002; Peng et al., 2006; Röper et al., 2000). Brij98 (polyoxyethylene(20) oleyl ether) has been used to purify detergent-insoluble rafts that are enriched in cholesterol, sphingolipids, and myristyolated/palmitoylated proteins, while solubilizing prenylated proteins, including the mammalian GTPase Rab5 (Drevot et al., 2002). Following

incubation at 4°C in the presence of 0.5% Brij98, wild-type vacuoles displayed only a mild solubilization of fusion proteins, with the exception of Ypt7p, which was consistent with results from previous studies. We were intrigued to see little change in the amount of membrane associate Rho1p, expecting to see a distribution that resembled that of Ypt7p **(Fig. 8B, WT, lanes 1 & 2 vs lanes 7-10)**. When *elo3*Δ vacuoles were subjected to the same detergent treatment, we found the membrane-embedded Vph1p, and membrane-associated actin was almost completely lost from the low-density membrane fractions and redistributed throughout the gradient. We also observed a decrease in membrane associated Ypt7p, however the heavy fractions which represent soluble proteins did not show a concomitant increase in a band at the same size, instead there was a noticeable increase in signal at a lower molecular weight, possibly representing a degradation product or a change in the degree of prenylation. We observed a similar, fast-migrating band in the soluble Rho1 fraction **(Fig. 8B, *elo3*Δ, lanes 1 & 2 vs lanes 7-10)**. Lubrol WX (polyoxyethelene(17) cetyl stearyl ether) has similarly been used to isolate membrane rafts of different protein and lipid composition than the Triton X-100 and Brij98 insoluble rafts (Röper et al., 2000). When isolated wild type vacuoles were incubated with 0.5% Lubrol WX, we observed a gradient distribution that was strikingly similar to that observed following Brij98 treatment **(Fig. 8C)**. Taken together, these results reinforce the idea that sphingolipids that contain VLCFAs are necessary to maintain raft composition at the vacuole, and the use of different mild detergents indicates that GTPases of different subfamilies may reside in different nanodomains.

The observations that purified vacuoles lacked normal fusion markers **(Fig. 3)**, small GTPases were lost from vacuolar subdomains **(Fig. 4)** and membrane proteins were easily solubilized **(Fig. 8A)** from *elo3*Δ vacuoles raised the possibility that this was due to altered membrane fluidity. To determine if the lack of a functional Elo3p alters the fluidity of vacuolar membranes, we used a Membrane Fluidity Kit (Marker Gene Inc.) to quantify this property. The literature suggests that biological membranes that display a higher ratio of excimer fluorescence versus monomer fluorescence are more fluid (liquid-disordered like) after being labeled with the pyrene-based dye (Galla and Luisetti, 1980; Tavolari et al., 2012). Vacuoles were incubated with the fluorescent probe and the ratio of the excimer/monomer fluorescence was measured **(Fig. 8D)**. As expected, vacuoles lacking C26 VLCFA-containing sphingolipids have a higher excimer/monomer fluorescence ratio, indicating they are more fluid than the wild-type vacuolar membranes. We attempted to couple this experimental setup with the presence of 0.5% Lubrol WX and Brij98, however these reactions produced very little excimer fluorescence, possibly due to micelle formation from lysed membranes. Thus, we conclude that yeast vacuoles require C26 VLCFAs to produce sphingolipids that create a more ordered membrane bilayer for proper retention and localization of fusogenic proteins.

Discussion

Here we show that yeast strains that are unable to produce C26 VLCFAs are unable to enrich the vertex region of docked vacuoles with a subset of fusion Rab and Rho GTPases, which causes a significant block in the tethering and docking steps of the fusion cascade. Previous studies performed by our group and others have focused on the glycerophospholids that are necessary to drive the vertex enrichment of fusion machinery proteins at the yeast vacuole (Fratti et al., 2004; Karunakaran et al., 2012; Wang et al., 2002), yet the function of sphingolipids in this process remained unclear. Studies have shown that C26 VLCFAs are found almost exclusively within sphingolipids at the amide bond position, leaving only trace amounts of free VLCFAs within the cell (Lester et al., 1993; Megyeri et al., 2016). They are often decorated with inositol and mannose sugar attachments at the head group, and the yeast vacuole has been shown to contain relatively high amounts of IPC (Hechtberger et al., 1994). Therefore, we speculate that the observations outlined in our work stem from a lack of C26-VLCFA-containing sphingolipids, as opposed to a lack of free cerotic acid. This speculation is enforced by the observation that cells treated with sphingolipid biosynthesis inhibitors display similar vacuolar morphology phenotypes to *elo3*Δ cells **(Fig. 1)**. Wild-type yeast produce sphingolipids that most often (70-90%) contain a C26:0:1 (cerotic acid with no double bonds, and a single hydroxylation within the acyl chain), whereas yeast that lack Elo3p have been shown to produce non-canonical sphingolipids with shorter acyl chains (20-24 carbons). This is accompanied by an alteration of the relative abundance of other known regulatory lipids (PtdInsP's and ergosterol), and a significant decrease in complex sphingolipid levels (Ejsing et al., 2009; Megyeri et al., 2016; Oh et al., 1997). In contrast, the bulk of the glycerol-based lipids, whose fatty acid chains are usually 16 or 18 carbons long, and typically contain one or two desaturated fatty acids (16:1 and/or 18:1), are less affected by the loss of Elo3p. Using an *ELO3* null strain it was found that sphingolipids containing VLCFAs also function upstream of the vacuole during Vps21p-related endosomal maturation (Obara et al., 2013). *Elo3*Δ strains of *S. cerevisiae* were found to contain fragmented vacuoles, which have been shown to lack a fully functional vacuolar ATPase (Chung et al., 2003; Kohlwein et al., 2001). Similarly, yeast strains depleted of Acb1p (acyl-CoA binding protein) were shown to produce less C26 VLCFAs and displayed multi-lobed vacuoles that lacked membrane-bound SNAREs. These vacuoles were also found to have less ceramide and IPC, and were fusion-deficient (Faergeman et al., 2004; Gaigg et al., 2001).

The observation that vacuoles isolated from cells lacking C26 VLCFAs are fusion deficient could arguably be attributed to either one or both of the following: biophysical requirements of the membrane – such as interdigitation of acyl chains, or strong hydrogen bonding (Haque et al., 2001; Peter Slotte, 2013); and/or sphingolipid-rich nanodomains at vertex regions that serve as platforms for fusion protein concentration and localized activity (Harayama and Riezman, 2018; Raghupathy et al., 2015; Sezgin et al., 2017). Indeed, the results obtained from lipid-mixing **(Fig. 2C)** are reminiscent of experiments that monitored the dequenching of NBD-labeled lipids into liposomes composed of lipids with specific acyl chain lengths (Molino et al., 2014). However, we could detect no significant block during pore formation between lipid and

content mixing **(Fig. 2D and 2E).** The striking differences in the relative amounts of vacuolar fusion proteins as determined by immunoblot **(Fig. 3)** and microscopic experiments **(Fig. 1)**, led us to investigate the protein and lipid composition of the well-studied fusion assembly. Previous studies have highlighted the trafficking defects of yeast that are deficient in C26 VLCFAs, which we confirmed and expanded upon in this study (Faergeman et al., 2004; Obara et al., 2013). We observed significant decreases of many fusion proteins that are normally trafficked to the vacuole, while the protein levels in whole cell lysates appeared similar **(Fig. 3)**, however mRNA expression levels were not directly investigated in this study. We were intrigued with the localization patterns of proteins that traffic to the vacuole via different routes, specifically Pho8p (alkaline phosphatase - ALP) and Prc1p (carboxypeptidase Y - CPY)/Pep4p (proteinase A - PrA), which reach the vacuole through the AP-3 and AP-1 (vacuolar protein sorting - VPS) pathways, respectively (Feyder et al., 2015). Pioneering work by Klionsky and Emr closely monitored the maturation and transit of Pho8p through the endomembrane system, which was instrumental in the discovery and characterization of the AP-3 pathway (Klionsky and Emr, 1989). Their work identified how Pho8p was situated within the vacuolar membrane and highlighted three major forms of the protein; pro-, mature, and soluble. While we did not observe any significant defect in traditional AP-3 trafficking to the vacuole (i.e. a buildup of the proPho8p due to a lack of processing by vacuole-resident proteases) we observed a significant increase the in the roughly 66 kDa soluble form of Pho8p **(Figs. 3 and 8, Pho8p immunoblots)**. This soluble form of Pho8p (sPho8p) has shown up in multiple studies with little to no mention of any biological significance (Anand et al., 2009; Faergeman et al., 2004; Klionsky and Emr, 1989; Obara et al., 2013). Similar to the work we have presented above, Obara *et al.* discovered a previously unknown relationship between Vps21p-mediated vesicular transport at the late endosome and VLCFA production (Obara et al., 2013). They also observed significant increases to the amount of sPho8p in *sur4*Δ (*elo3*Δ) cells. Faergeman *et al.* also worked with yeast that had significantly reduced C26 VLCFA content, albeit from a depletion of Acb1p as opposed to a loss of Elo3p, which also showed an increase in this sPho8p (Faergeman et al., 2004). To this point we have only found one published study that investigated the biological significance of this soluble form of vacuolar alkaline phosphatase, and together with our work and the studies referenced above, may help to describe some of the pleiotropic effects observed following the of a loss of C26 VLCFAs. Work by Linsheng Song showed that the sPho8p has biological significance as a farnesyl diphosphate (FPP) phosphatase (Song, 2006). This allows us to speculate about the cause of two observations outlined in our presented work, both of which stem from a decrease in the availability and/or recycling of FPP. FPP is the precursor to squalene synthesis, which is necessary for the biosynthesis of sterols. We have shown that vacuoles isolated from *elo3*Δ yeast are still able to enrich ergosterol at the vertex region of docked vacuoles **(Fig. 7B)**, even though they have been shown to produce less ergosterol and have disrupted microdomain formation in vacuole membranes (Ejsing et al., 2009; Klose et al., 2010). FPP is also the precursor to geranylgeranyl diphosphate (GGPP), which is the co-substrate for the prenylation of Rab (Vps21p/Ypt7p) and Rho (Cdc42p/Rho1p) family GTPases, and is necessary for sustained membrane localization and activity of these proteins (Ingolfsson et al., 2007; Langemeyer et al., 2018). We have shown that GTPases

are lost from the vacuolar membrane **(Fig. 3)** and fail to enrich at the vertex of docked vacuoles **(Fig. 5)**. We also observed a downshift in the apparent molecular weight of Ypt7p on isolated vacuoles from the *elo3*Δ strain when we tested the detergent insolubility of fusion proteins **(Fig. 8).** This shift in molecular weight could be a degradation product formed by a buildup of unprenylated Ypt7p, as the intense upper band is consistent with the doubly prenylated form of the protein (Langemeyer et al., 2018; Thomä et al., 2001). These speculations will require a significant amount of work to investigate, but it provides a link between the abundance of VLCFAs and sPho8p, and the production of prenylated GTPases. We also detected minor increases in the amount of the pro-forms of Pep4p (PrA) and Prc1p (CPY) in cells lacking VLCFAs, but these proteases still reach full maturation states in *elo3*Δ yeast, which reflects results that had been previously shown in other studies **(Fig. 3)** (Obara et al., 2013).

As mentioned above, Cdc42p and Rho1p, two Rho-family GTPases, play distinct but similar roles in the regulation of actin polymerization at the yeast vacuole. When Cdc42p at the vacuole is in its active GTP-bound state it activates Las17p (yeast homolog of WASP), which in turn activates Arp2p/Arp3p-mediated actin polymerization to bring vacuoles in close proximity (Eitzen et al., 2002). The contribution of Rho1p to the final steps in fusion is less clear, but recent work suggests that Rho1p-GDP interacts with a pool of vacuole associated Tef1p/Tef2p (eEIFα). This complex dissociates upon Rho1p binding to GTP, allowing Tef1p/Tef2p to bundle actin filaments, maintaining membrane integrity during and after fusion (Bodman et al., 2015). Cdc42p localization and activation at the plasma membrane has been shown to be dependent on membrane curvature, effector proteins, and phosphatidylserine (PS), and its activity at the vacuole is known to depend on ergosterol levels (Jones et al., 2010; Sartorel et al., 2018; Smith et al., 2017),96). In both the mammalian and yeast systems many Rho-family GTPases also contain polybasic regions (PBRs) within the C-terminal hypervariable region. These hypervariable regions have been shown to facilitate interactions between small GTPases and membrane lipids including PtdIns(4,5)P_2 (a positive regulator of vacuolar fusion), and strongly influence the specific subcellular location of Rho proteins (Kilchert and Spang, 2011; Michaelson et al., 2001). Some mammalian members of the Rho subfamily of GTPases are palmitoylated at cysteine residues, a transient post-translational modification that has been shown to drive some proteins to DRMs or lipid rafts which are enriched in sterols, sphingolipids, and other lipids with saturated acyl chains (Resh, 2016). Rho3p has been shown to be palmitoylated, which is a major determinant in its distinct localization relative to Cdc42p at the plasma membrane (Wu and Brennwald, 2010). One outstanding question still remains when thinking about Cdc42p/Rho1p localization; what drives their differential localization to PM or the vacuole? The activities of the three Rho1p GEFs Rom1p, Rom2p, and Tus1p have been investigated, but mostly in the context of cell division (Krause et al., 2012; Ozaki et al., 1996). Tus1p has been shown to activate the ABCC transporter Ycf1p, but it is currently unknown if this interaction plays a role in homotypic vacuole fusion (Paumi et al., 2007). The answer will most likely lie somewhere within cell-cycle expression of the proteins they interact with (i.e. GEFs and/or GAPs), of which there are many in the literature. While we isolate purified vacuoles to monitor their homotypic fusion, we must remind

ourselves that this process serves two major purposes in the context of the *in vivo* cell: vacuole inheritance by the daughter cell following division, and the fusion of vacuoles that have undergone fission events following the recovery from osmotic insults (Weisman, 2003). It's reasonable that a subset of GTPase interacting proteins are localized to the PM, while another subset is localized to the vacuole, allowing for the correct timing of cellular division and vacuole inheritance. Future studies will aim to investigate any potential direct interactions between small GTPases, effector proteins, and sphingolipids.

It was initially shown that lipids isolated from yeast can form model membranes that separate into visibly distinct domains when they were labeled with fluorescent lipophilic dyes with different lipid-partitioning properties (Klose et al., 2010). The domain that was found to be liquid-ordered-like (L_o-like) was enriched in BODIPY-cholesterol, and this domain dissipated and was visually absent when the lipids were isolated from yeast lacking a functional Elo3p enzyme. This phase separation in yeast lipids was demonstrated again when it was shown that when yeast cells are grown to stationary phase the vacuole membrane displays regions that separate into distinct lipid domains *in vivo* (Toulmay and Prinz, 2013). These domains were found to be enriched in either Vph1p (component of the V-ATPase) or Ivy1p (PtdIns(3,5)P_2-binding protein that interacts with Ypt7p and Vps33p), and they display properties that are indicative of differences in relative membrane fluidity. Fluorescently tagged Vph1p colocalizes with a dye that partitions into liquid-disordered-like (L_d-like) membranes, while a fluorescent Ivy1p construct colocalizes with the macrolide filipin III, which binds to ergosterol in yeast membranes in the liquid-ordered-like (L_o-like) region of the membrane. We monitored the vacuolar distribution of the proteins Vph1p and Ypt7p after density separation in the absence and presence of mild non-ionic detergents **(Fig. 8)**. In the absence of detergent, we expect little to no lysis of the purified vacuoles, which implies that the bottom-heavy fractions represent free soluble proteins that show little affinity towards the vacuole membrane, and/or a population of very dense vesicles. Microscopic analyses of *elo3*Δ would suggest that it is likely a mixture of both phenomena. When the *ELO3* gene is deleted we noticed a buildup of vesicles that cluster around a center vacuole (Class F morphology) **(Fig. 1)**, and fluorescence signal of chimeric small GTPases (Rho1p and Ypt7p) appeared more diffuse throughout the cytoplasm **(Fig. 5)**. There was a pronounced shift towards soluble forms of every protein of interest except for Rho1p, which showed a modest shift towards the soluble fraction of *elo3*Δ vacuoles, before the addition of any detergent **(Figure 8, top panels)**. Following incubation of the *elo3*Δ vacuoles with either detergent significantly ablated the membrane association of every protein of interest, which we interpret as a solubilization of the predominantly L_d-like membranes that form when sphingolipids are absent. Interestingly, Rho1p signaling at the PM has been linked to membrane fluidity before (Lockshon et al., 2012), and our results point to a possible signaling loop, wherein Rho1p and its effectors sense membrane fluidity of multiple membrane systems.

As mentioned above, Vph1p and Ivy1p have been used as markers for the L_d-like and L_o-like regions of the vacuole membrane respectively (Toulmay and Prinz, 2013). Vph1p localization was subsequently utilized

as a negative marker in studies to show that the regulatory fusion lipids PtdIns(3)P, PtdIns(4)P, and PtdIns(3,5)P_2 tend to be enrich in regions that lack Vph1p and intramembrane particles (IMPs) (Takatori et al., 2016; Tomioku et al., 2018), i.e. these known regulatory lipids enrich in the raft-like domains that are also known to contain relatively high amounts of sphingolipids and sterols. However, it should be noted that other studies have demonstrated an activation of the V-ATPase upon the addition of exogenous, short-chain PtdIns(3,5)P_2 and a stabilization of the V_O-V_1 complex by this lipid, suggestive of a protein-lipid interaction (Li et al., 2014). There has recently been significant work in uncovering the mechanism and function of the formation of intralumenal fragments (ILFs) following homotypic vacuolar fusion (Karim et al., 2018; Mattie et al., 2017; McNally et al., 2017). The formation and visualization of ILFs is possible when stalk expansion and pore formation takes place very quickly following the formation of the hemifusion diaphragm, and when the rate of hemifusion is slowed down, the ILFs do not form. The biological function of ILF formation has been determined to be a pathway for the turnover of membrane-embedded vacuolar transporters and membrane lipids. The observation that that some polytopic membrane proteins are enriched (Fth1p, Cot1p, Sna4p), excluded (Fet5p, Ycf1p, Ybt1p, Ncr1p), or uniformly distributed (Vph1p) into the boundary region for ILF production and degradation raises the possibility that physical properties of the membrane (such as inclusion or exclusion from lipid rafts) could play a role in this new sorting process at the yeast vacuole. We are currently investigating if the lack of C26 VLCFA containing sphingolipids alters the sorting of these polytopic proteins into the boundary region for eventual ILF formation and degradation.

Materials and Methods

Yeast strains and growth conditions

Yeast strains and primers used in this study are found in Table 1 and Table 2, respectively. Yeast strains were grown in YPD [1% yeast extract, 2% peptone, 2% dextrose (RPI)], or synthetic drop-out media [YNB lacking amino acids and ammonium sulfate (RPI), with amino acids, adenine, and uracil (Millipore-Sigma) added at ~76 mg/L, except leucine which was at ~380 mg/L, RPI) lacking the specified nutrient the specified nutrient. The *ELO3* coding sequence was deleted using homologous recombination by amplifying the *hphMX6* gene conferring hygromycin resistance from the vector pAG32 (Addgene) using the primers elo3F and elo3R (IDT). The PCR product designed for homologous recombination was transformed using lithium acetate (Sigma) as previously described (Tripp et al., 2013), and cells were grown on YPD agar (RPI) plates containing 200 mg/L hygromycin B (Goldbio). The high expression dsRed-Rho1 vector was created using the splicing by overlap extension method (Higuchi et al., 1988). Briefly, the TEF promoter sequence was amplified from the pAG32 vector using the primers TEF F and TEF R, creating KpnI and XmaI sites and the 5' and 3' ends respectively, and inserted into the pRS416 (Stratagene) vector following digestion with KpnI/XmaI (Christianson et al., 1992; Sikorski and Hieter, 1989). The dsRed monomer was amplified from the DsRed-Monomer Vector (Takara) using the primers dsR F and dsR R creating a 5' XmaI site and a 3' region homologous to the 5' region of Rho1, The Rho1 gene was amplified using the primers Rho1 F and

Rho1 R creating a 5' region with homology to the 3' end of dsRed-Monomer and a 3' SacI site. These PCR products were mixed, and amplified again using the primer s dsR F and Rho1 R. The final product was cut using XmaI/SacI and inserted into the pRS416-TEF vector. All enzymes used for DNA manipulation and subcloning were purchased from New England Biolabs. The construct was confirmed via sequencing (ACGT). pRS424GFP-FYVE(EEA1) was purchased from Addgene. All plasmids were transformed into BJ3505 wild-type and *elo3*Δ strains via electroporation (BIORAD) and plated onto appropriate auxotrophic selection plates.

Live microscopy

General vacuolar morphology of live yeast was determined by growing cells overnight in YPD at 30°C to mid-log phase. Cells were then diluted in fresh YPD to OD of 0.6 and allowed to grow for another hour, before treatment with 0.25 µg/mL myriocin (Cayman), 0.125 µg/mL aureobasidin A (Takara), 50 µM cerulenin (Cayman), or methanol (Macron) vehicle control. After additional growth in the presence of inhibitor for ~5 hours, Yeast Vacuole Membrane Marker MDY-64 (Thermo Fisher) was added to a final concentration of 10 µM, and cells were incubated at 30°C for 15 minutes. Cells were then isolated by centrifugation (12000 x g, 1 min, room temperature) and resuspended in PBS. Twenty microliters of this cell suspension was then mixed 1:1 with 0.6% low-melt agarose (RPI) warmed to 50°C, and 10 µL of the mixture was placed on a glass slide (AmScope) and covered with a glass coverslip (Thermo) for viewing by fluorescence microscopy. For strains expressing a fluorescent construct, overnight growth was in SC dropout media for plasmid maintenance before cells were back diluted into YPD. For strains expressing a green fusion protein, the cells were grown in the presence of 10 µM FM4-64 (Thermo Fisher) for the ~6 hours following back dilution, while those that expressed red fusion proteins were incubated with 10 µM Yeast Vacuole Marker MDY-64 (Thermo Fisher) for the final 20 minutes prior to visualization. Images were acquired using a Zeiss Axio Observer Z1 microscope equipped with an X-Cite 120XL light source, Plan Apochromat x63 oil objective (NA 1.4) and an AxioCam CCD camera. All images were analyzed with ImageJ software (NIH).

Vacuole isolation and in vitro content mixing

Yeast vacuoles were isolated as previously described (Haas et al., 1994) with slight modifications. Yeast were grown to OD_{600} values of 0.7-1.1, cells were washed with 50 mL of 100 mM Tris-Cl (Thermo Fisher), pH 9.4, 15 mM DTT (RPI), and incubated at room temp for 10 minutes. Following wash, the cells were kept in spheroplasting buffer with oxalyticase for 45 minutes before spinning for 10 min at 1000 x g. All other steps in vacuole isolation were identical as referenced. Content mixing reactions (30 µL) contained 3 µg each of vacuoles from BJ3505 (*pep4*Δ *PHO8)* and DKY6281 (*PEP4 pho8*Δ) backgrounds, fusion reaction buffer [20 mM PIPES-KOH (Sigma), pH 6.8, 200 mM sorbitol (RPI), 125 mM KCl (RPI), 5 mM $MgCl_2$ (Sigma)], ATP regenerating system [1 mM ATP (RPI), 0.1 mg/mL creatine kinase (Sigma), 29 mM creatine phosphate (Abcam)], 10 µM CoA (Sigma), and 280 nM Pbi2 (IB_2, PrB inhibitor). Reactions were incubated at 27°C and Pho8p activity was assayed in 250 mM Tris-Cl, pH 8.5, 0.4% Triton X-100 (RPI), 10 mM $MgCl_2$,

1 mM *p*-nitrophenylphosphate (MP Biomedicals). Fusion was monitored as the absorbance at 400 nm from *p*-nitrophenolate production through phosphatase activity.

Lipid mixing

Lipid mixing assays were performed as previously described for vacuolar outer leaflet mixing (Qiu and Fratti, 2010). Vacuoles were isolated from BJ3505 background yeast (300 µg) and then labeled by incubating with 400 µL of PS buffer (10 mM PIPES-KOH pH 6.8, 200 mM sorbitol) containing 150 µM rhodamine B DHPE (Rh-PE; Thermo Fisher) by nutation for 10 minutes at 4°C. Following labeling, 800 µL of 15% Ficoll 400 (Bio Basic) (in PS buffer) was mixed with the vacuoles and transferred to 11 x 60 mm polyallomer ultracentrifuge tube, overlaid with 1.2 mL of 8% Ficoll, 1.2 mL of 4% Ficoll, and 0.5 mL of PS buffer. Vacuoles were separated from free dye by centrifugation (100,000 x g, 25 min, 4°C, SW-60 Ti rotor, Beckman L8-80M Ultracentrifuge) and recovered from the 0%-4% interface. Lipid mixing reactions (90 µL) contained 2 µg of labeled vacuoles and 16 µg of unlabeled vacuoles in fusion reaction buffer (20 mM PIPES-KOH, pH 6.8, 200 mM sorbitol, 125 mM KCl, 5 mM $MgCl_2$), ATP regenerating system (1 mM ATP, 0.1 mg/mL creating kinase, 29 mM creatine phosphate), 10 µM CoA, and 280 nM Pbi2 (IB_2, PrB inhibitor). Reaction mixtures were transferred to a black, half-volume, 96-well flat-bottom microtiter plate (Corning), and fluorescence from dequenching was monitored (λ_{ex}=544 nm, λ_{em}=590 nm) in a POLARstar Omega BMG Labtech plate reading fluorometer. Readings were taken every minute for 60 minutes at 27°C. The data shown is normalized to the wild type reading at 60 minutes.

Docking experiments

Vacuoles isolated as outline above were subjected to docking assays as previously described (Fratti et al., 2004; Wang et al., 2002) with slight modifications. Docking reactions (30 µL) contained 6 µg of vacuoles isolated from the indicated strains in docking reaction buffer (100 mM KCl, 0.5 mM $MgCl_2$, 20 mM PIPES-KOH, pH 6.8, 200 mM sorbitol), 0.33X ATP regeneration system (0.33 mM ATP, 13 mM creatine phosphate, 33 µg/mL creatine kinase), 10 µM coenzyme A, and 280 nM Pbi2. Docking reactions between vacuoles expressing GFP fusion proteins or containing 5 µM Filipin III (Cayman) were incubated with 4 µM FM4-64. Reactions between vacuoles expressing dsRed or mCherry fusion proteins, or those including 0.25 µM Cy3-FYVE, were incubated with 0.5 µM Yeast Vacuole Membrane Marker MDY64. Recombinant GDI and Cy3-FYVE domain were purified and utilized in docking reactions as previously described (Eitzen et al., 2002; Wang et al., 2002), following labeling with Cy3 dye (GE Healthcare). Following incubation in the dark at 27°C for 20 minutes, reactions were mixed with 30 µL of 0.6% low melt agarose in PS buffer melted at 50°C, and 10 µL aliquots were mounted on pre-chilled slides and observed by fluorescence microscopy. Images were acquired using a Zeiss Axio Observer Z1 microscope equipped with an X-Cite 120XL light source, Plan Apochromat x63 oil objective (NA 1.4) and an AxioCam CCD camera. Exposure times were held constant within an experiment. All images were analyzed using ImageJ software (NIH).

Swept-field microscopy

Wild type or elo3Δ yeast cells expressing Abp1-mCherry were grown for 17 h in synthetic complete medium lacking tryptophan (SC –TRP). Cells were then harvested, washed and resuspended in fresh YPD medium, and incubated at 30°C for 3 h. Vacuoles were then labeled with MDY-64 (final concentration 23 µM) using a pulse-chase method replacing FM4-64 (Vida and Emr, 1995) whereby cells were resuspended in SC –TRP and plated on concavalin-A coated coverslips (1 mg/mL in 50 mM HEPES pH 7.5, 20 mM calcium acetate, 1 mM $MnSO_4$). Time-lapse videos were acquired over 2 min at room temperature using a Nikon Livescan swept-field confocal fluorescence microscope equipped with an Agilent MLC400 Monolithic laser combiner unit (housing 100 mW 488 nm and 561 nm lasers), Andor Ixon3 EMCCD camera, and Nikon CFI Plan Apo Lambda 1.49 NA 100 x objective lens, operated with Nikon Elements software. Videos were processed using ImageJ software to subtract background noise, invert single channel images, and to prepare 3-D intensity plots. Then an unsharpen mask was applied using Adobe Photoshop prior to assembly into figures using Adobe Illustrator software.

Calcium efflux

Calcium efflux assays were performed as described with minor modifications (Miner and Fratti, 2019). Briefly, fusion reactions (60 µL) containing 20 µg of purified vacuoles were incubated in fusion reaction buffer containing 150 nM of Cal-520 (AAT Bioquest). Anti-Sec17 IgG was added at a concentration of 80 µg/mL to inhibit calcium efflux, and was purified as previously described (Mayer et al., 1996). Reaction mixtures were transferred into a black, half-volume 96-well flat-bottom plate with nonbinding surface. ATP regenerating system or PS buffer was added, and the fluorescence was monitored at 27°C (λ_{ex}=485 nm, λ_{em}=520 nm) using a POLARstar Omega BMG Labtech plate reading fluorometer for 45 minutes.

Immunoblotting

To detect fusion proteins from whole cell extracts, TCA precipitation was performed as described in (Karim et al., 2018) with slight modification. Briefly, 10 OD units of log phase cells (corresponding to OD600 of 0.8-1.2) grown overnight in YPD were collected and subjected to lysis [0.2 M NaOH (VWR), 0.2% β-mercaptoethanol (Sigma)] and chilled on ice for 10 minutes. Fifty percent Trichloroacetic acid solution (Alfa Aesar) was added to a final concentration of 5% and samples were placed on ice for 10 minutes. Precipitates collected by centrifugation (12000 x g, 5 min, 4°C), washed in ice-cold acetone, and again collected by centrifugation (12000 x g, 5 min, 4°C). Samples were resuspended in 200 µL of dissociation buffer [4% SDS (Thermo Fisher), 0.1 M Tris-Cl pH 6.8, 4 mM EDTA (Thermo Fisher), 20% glycerol (Thermo Fisher), 2 % β-mercaptoethanol (Sigma), and 0.02% bromophenol blue (Sigma)]. Tris-Cl pH 6.8 was added to a final concentration of 0.3 M and samples were boiled for 5 min at 90°C. Five microliters (corresponding to ~0.11 OD units of cells) of protein sample were loaded onto 10% SDS-PAGE gels (90 V, 120 min), and transferred to 0.2 µm nitrocellulose membranes (BIORAD) at 10 V overnight. Transferred proteins were blocked in 6% milk solution, incubated with primary antibody for ~12 hours, washed with PBST, and

incubated with secondary antibody [goat anti-rabbit or goat anti-mouse Dylight 650, (Invitrogen Thermo Fischer)] for one hour to visualize. Primary antibodies utilized for this study were used as previously described (Bodman et al., 2015; Haas et al., 1995; Haas and Wickner, 1996; Mayer and Wickner, 1997; Peng et al., 2006; Price et al., 2000; Seals et al., 2000)

Proton pumping

The proton pumping activity of purified yeast vacuoles was performed as described with modifications (Müller et al., 2003). Proton transport reactions (60 µL) contained a mixture of 20 µg of purified vacuoles from the indicated strain, 10 µM CoA, 283 nM Pbi2 and 15 µM acridine orange (Thermo Fisher). Reaction mixtures were loaded into a black, half-volume 96-well flat-bottom plate with nonbinding surface. ATP regenerating system (1 mM ATP, 0.1 mg/mL creatine kinase, 29 mM creatine phosphate) or PS buffer was added, and reactions were incubated at 27°C while fluorescence was monitored (λ_{ex}=485 nm, λ_{em}=520 nm) in a POLARstar Omega BMG Labtech plate reading fluorometer. The V-ATPase activity was specifically inhibited with 50 µM Bafilomycin A1 (Cayman). Reactions were initiated by the addition of ATP regeneration system following and initial measurement. After 10 minutes of incubation and fluorescence dequenching, FCCP (carbonyl cyanide-4-(trifluoreomethoxy)phenylhydrazone) (Cayman) was added (30 µM final concentration) to collapse the proton gradient and restore acridine orange fluorescence.

DRM isolation

Detergent resistant membranes were isolated from vacuoles by modifying the methods from previous studies (Bagnat et al., 2000; Peng et al., 2006). Yeast vacuoles were harvested as outlined above. Following isolation, 270 µL of 0.33 mg/mL vacuoles in PS buffer were gently mixed with 30 µL of 10% Triton X-100, 5% Brij98 (ACROS Organics), 5% Lubrol WX (MP Biomedicals), or PS buffer to reach the desired composition (0.5-1%). The mixture were incubated at 4°C for 30 minutes before mixing with 550 µL of 60 % Optiprep (Sigma). Next, 1.2 mL of 30% Optiprep and 200 µL of 0% Optiprep (diluted in PS buffer) were layered on top of the detergent mixture. The gradients were centrifuged (2.5 h at ~160000xg in a SW60 Ti rotor at 4°C), and ten (200 µL) fractions were taken from the top. Fifteen microliters of each sample was loaded for subsequent SDS-PAGE and immunoblot analyses.

Pyrene-actin polymerization assay

The *in vitro* pyrene-actin assay was performed as previously described (Isgandarova et al., 2007). Briefly, vacuoles were isolated from BJ3505 background yeast and 7X fusion reactions (corresponding to 42 µg of isolated vacuoles in a 210 µL reaction) in fusion reaction buffer (20 mM PIPES-KOH, pH 6.8, 200 mM sorbitol, 125 mM KCl, 5 mM $MgCl_2$) were preincubated at 27°C for 30 minutes. After preincubation, 200 µL of PS buffer was added to the reactions, they were briefly vortexed, and then spun down (12000xg, 5 minutes, 4°C). Vacuole pellets were resuspended in 70 µL of G-Buffer/NP/Mg [5 mM Tris-HCl, pH 8, 0.2 mM $CaCl_2$ (Sigma), 0.2 mM ATP, 0.17% Nonidet P-40 (Fluka), 0.35 mM $MgCl_2$], and mixed with 50 µL of

12 µM pyrene muscle actin (Cytoskeleton Inc.) in G-Buffer (5 mM Tris-HCl, pH 8, 0.2 mM $CaCl_2$, 0.2 mM ATP). Next, 100 µL of this mixture was immediately added to wells in a black, half-volume, 96-well flat-bottom microtiter plate and fluorescence was monitored (λ_{ex}=355 nm, 410 nm, 180 cycles, 20 second cycles, 27°C, POLARstar Omega BMG Labtech plate reader). Reactions were blanked against a PS buffer + pyrene muscle actin (5 µM) well.

Membrane fluidity assay

Membrane fluidity kit (Marker Gene) was used following manufacturer's instructions. Briefly, vacuoles isolated from BJ3505 wild-type or *elo3*Δ cells (25 µg total protein diluted to 50 µL in PS buffer, 0.5 mg/mL final) were mixed with the pyrenedecanoic acid (PDA) in 10 mM PIPES-KOH pH6.8, 200 mM sorbitol (PS) (50 µL of a 20 µM PDA stock in PS + 0.08% Pluronic F127) in a 100 µL reaction. This mixture was left to incubate in the dark for 20 minutes before being spun down 5000xg for 5 minutes at room temp, and resuspended in 100 µL of PS. Resuspended mixtures were put in a black half-volume, flat-bottom 96-well plate and endpoint fluorescent emission was measured (λ_{ex}=355 nm, $\lambda_{em(monomer)}$=410 nm, and $\lambda_{em(excimer)}$=520 nm, POLARstar Omega BMG Labtech). Samples of isolated vacuoles were blanked against a mixture of 50 µL 20 µM PDA in PS + 0.08% Pluronic F127 and 50 µL PS.

Acknowledgements

The authors wish to thank Dr. Lois Weisman, Dr. Gary Eitzen, and Dr. William Wickner for the generous gifts of primary antibodies and antisera. We also thank Dr. Anne Spang for gifting the p414-ADH1-N17-2xmCherry plasmid. We thank members of the Fratti lab for help with experiments and discussions, especially Dr. Matt Starr, for his invaluable help in creating the dsRed-Rho1p plasmid. The authors thank C. Law and the Centre for Microscopy and Cellular Imaging at Concordia University for assistance with swept-field microscopy. This research was supported by grants from the National Institutes of Health (R01-GM101132) and National Science Foundation (MCB 18-18310) to RAF, and Natural Sciences and Engineering Research Council of Canada grant RGPIN/2017-06652 to CLB.

Author contributions: LRH and RAF, Conception and design, Data analysis and interpretation, Drafting or revising the article; LRH, CZ, TK, DAR-K, CLB and RAF Acquisition of data, data analysis.

The authors declare no competing financial interests

References

Abe, M., H. Qadota, A. Hirata, and Y. Ohya. 2003. Lack of GTP-bound Rho1p in secretory vesicles of Saccharomyces cerevisiae. *J Cell Biol.* 162:85-97.

Anand, V. C., L. Daboussi, T. C. Lorenz, and G. S. Payne. 2009. Genome-wide analysis of AP-3-dependent protein transport in yeast. *Mol Biol Cell.* 20:1592-1604.

Anderson, R. G., and K. Jacobson. 2002. A role for lipid shells in targeting proteins to caveolae, rafts, and other lipid domains. *Science.* 296:1821-1825.

Bagnat, M., S. Keranen, A. Shevchenko, A. Shevchenko, and K. Simons. 2000. Lipid rafts function in biosynthetic delivery of proteins to the cell surface in yeast. *Proc Natl Acad Sci U S A.* 97:3254-3259.

Bodman, J. A., Y. Yang, M. R. Logan, and G. Eitzen. 2015. Yeast translation elongation factor-1A binds vacuole-localized Rho1p to facilitate membrane integrity through F-actin remodeling. *J Biol Chem.* 290:4705-4716.

Brown, D. A., and J. K. Rose. 1992. Sorting of GPI-anchored proteins to glycolipid-enriched membrane subdomains during transport to the apical cell surface. *Cell.* 68:533-544.

Christianson, T. W., R. S. Sikorski, M. Dante, J. H. Shero, and P. Hieter. 1992. Multifunctional yeast high-copy-number shuttle vectors. *Gene.* 110:119-122.

Chung, J. H., R. L. Lester, and R. C. Dickson. 2003. Sphingolipid requirement for generation of a functional v1 component of the vacuolar ATPase. *J Biol Chem.* 278:28872-28881.

Collins, K. M., and W. T. Wickner. 2007. Trans-SNARE complex assembly and yeast vacuole membrane fusion. *Proc Natl Acad Sci U S A.* 104:8755-8760.

Conradt, B., A. Haas, and W. Wickner. 1994. Determination of four biochemically distinct, sequential stages during vacuole inheritance in vitro. *J Cell Biol.* 126:99-110.

Conradt, B., J. Shaw, T. Vida, S. Emr, and W. Wickner. 1992. In vitro reactions of vacuole inheritance in Saccharomyces cerevisiae. *J Cell Biol.* 119:1469-1479.

Denic, V., and J. S. Weissman. 2007. A molecular caliper mechanism for determining very long-chain fatty acid length. *Cell.* 130:663-677.

Desfarges, L., P. Durrens, H. Juguelin, C. Cassagne, M. Bonneu, and M. Aigle. 1993. Yeast mutants affected in viability upon starvation have a modified phospholipid composition. *Yeast.* 9:267-277.

Drevot, P., C. Langlet, X. J. Guo, A. M. Bernard, O. Colard, J. P. Chauvin, R. Lasserre, and H. T. He. 2002. TCR signal initiation machinery is pre-assembled and activated in a subset of membrane rafts. *EMBO J.* 21:1899-1908.

Eitzen, G., L. Wang, N. Thorngren, and W. Wickner. 2002. Remodeling of organelle-bound actin is required for yeast vacuole fusion. *J Cell Biol.* 158:669-679.

Eitzen, G., N. Thorngren, and W. Wickner. 2001. Rho1p and Cdc42p act after Ypt7p to regulate vacuole docking. *Embo J.* 20:5650-6.

Eitzen, G., E. Will, D. Gallwitz, A. Haas, and W. Wickner. 2000. Sequential action of two GTPases to promote vacuole docking and fusion. *Embo J.* 19:6713-20.

Ejsing, C. S., J. L. Sampaio, V. Surendranath, E. Duchoslav, K. Ekroos, R. W. Klemm, K. Simons, and A. Shevchenko. 2009. Global analysis of the yeast lipidome by quantitative shotgun mass spectrometry. *Proc Natl Acad Sci U S A.* 106:2136-2141.

Faergeman, N. J., S. Feddersen, J. K. Christiansen, M. K. Larsen, R. Schneiter, C. Ungermann, K. Mutenda, P. Roepstorff, and J. Knudsen. 2004. Acyl-CoA-binding protein, Acb1p, is required for normal vacuole function and ceramide synthesis in Saccharomyces cerevisiae. *Biochem J.* 380:907-918.

Feyder, S., J. O. De Craene, S. Bär, D. L. Bertazzi, and S. Friant. 2015. Membrane trafficking in the yeast Saccharomyces cerevisiae model. *Int J Mol Sci.* 16:1509-1525.

Fratti, R. A., Y. Jun, A. J. Merz, N. Margolis, and W. Wickner. 2004. Interdependent assembly of specific regulatory lipids and membrane fusion proteins into the vertex ring domain of docked vacuoles. *J Cell Biol.* 167:1087-1098.

Gaigg, B., T. B. Neergaard, R. Schneiter, J. K. Hansen, N. J. Faergeman, N. A. Jensen, J. R. Andersen, J. Friis, R. Sandhoff, H. D. Schrøder, and J. Knudsen. 2001. Depletion of acyl-coenzyme A-binding protein affects sphingolipid synthesis and causes vesicle accumulation and membrane defects in Saccharomyces cerevisiae. *Mol Biol Cell.* 12:1147-1160.

Galla, H. J., and J. Luisetti. 1980. Lateral and transversal diffusion and phase transitions in erythrocyte membranes. An excimer fluorescence study. *Biochim Biophys Acta.* 596:108-117.

Gillooly, D. J., I. C. Morrow, M. Lindsay, R. Gould, N. J. Bryant, J. M. Gaullier, R. G. Parton, and H. Stenmark. 2000. Localization of phosphatidylinositol 3-phosphate in yeast and mammalian cells. *Embo J.* 19:4577-88.

Haas, A., B. Conradt, and W. Wickner. 1994. G-protein ligands inhibit in vitro reactions of vacuole inheritance. *J Cell Biol.* 126:87-97.

Haas, A., D. Scheglmann, T. Lazar, D. Gallwitz, and W. Wickner. 1995. The GTPase Ypt7p of Saccharomyces cerevisiae is required on both partner vacuoles for the homotypic fusion step of vacuole inheritance. *Embo J.* 14:5258-70.

Haas, A., and W. Wickner. 1996. Homotypic vacuole fusion requires Sec17p (yeast alpha-SNAP) and Sec18p (yeast NSF). *Embo J.* 15:3296-305.

Haque, M. E., T. J. McIntosh, and B. R. Lentz. 2001. Influence of lipid composition on physical properties and peg-mediated fusion of curved and uncurved model membrane vesicles: "nature's own" fusogenic lipid bilayer. *Biochemistry.* 40:4340-4348.

Harayama, T., and H. Riezman. 2018. Understanding the diversity of membrane lipid composition. *Nat Rev Mol Cell Biol.* 19:281-296.

Hashida-Okado, T., A. Ogawa, M. Endo, R. Yasumoto, K. Takesako, and I. Kato. 1996. AUR1, a novel gene conferring aureobasidin resistance on Saccharomyces cerevisiae: a study of defective morphologies in Aur1p-depleted cells. *Mol Gen Genet.* 251:236-244.

Hechtberger, P., E. Zinser, R. Saf, K. Hummel, F. Paltauf, and G. Daum. 1994. Characterization, quantification and subcellular localization of inositol-containing sphingolipids of the yeast, Saccharomyces cerevisiae. *Eur J Biochem.* 225:641-649.

Higuchi, R., B. Krummel, and R. K. Saiki. 1988. A general method of in vitro preparation and specific mutagenesis of DNA fragments: study of protein and DNA interactions. *Nucleic Acids Res.* 16:7351-7367.

Ingolfsson, H. I., R. E. Koeppe, 2nd, and O. S. Andersen. 2007. Curcumin is a modulator of bilayer material properties. *Biochemistry.* 46:10384-10391.

Isgandarova, S., L. Jones, D. Forsberg, A. Loncar, J. Dawson, K. Tedrick, and G. Eitzen. 2007. Stimulation of actin polymerization by vacuoles via Cdc42p-dependent signaling. *J Biol Chem.* 282:30466-30475.

Jaffe, A. B., and A. Hall. 2005. Rho GTPases: biochemistry and biology. *Annu Rev Cell Dev Biol.* 21:247-269.

Johansen, J., V. Ramanathan, and C. T. Beh. 2012. Vesicle trafficking from a lipid perspective: Lipid regulation of exocytosis in Saccharomyces cerevisiae. *Cell Logist.* 2:151-160.

Jones, E. W., G. S. Zubenko, and R. R. Parker. 1982. PEP4 gene function is required for expression of several vacuolar hydrolases in Saccharomyces cerevisiae. *Genetics.* 102:665-677.

Jones, L., K. Tedrick, A. Baier, M. R. Logan, and G. Eitzen. 2010. Cdc42p is activated during vacuole membrane fusion in a sterol-dependent subreaction of priming. *J Biol Chem.* 285:4298-4306.

Jun, Y., and W. Wickner. 2007. Assays of vacuole fusion resolve the stages of docking, lipid mixing, and content mixing. *Proc Natl Acad Sci U S A.* 104:13010-13015.

Karim, M. A., E. K. McNally, D. R. Samyn, S. Mattie, and C. L. Brett. 2018. Rab-Effector-Kinase Interplay Modulates Intralumenal Fragment Formation during Vacuole Fusion. *Dev Cell.* 47:80-97.e6.

Karunakaran, S., and R. Fratti. 2013. The Lipid Composition and Physical Properties of the Yeast Vacuole Affect the Hemifusion-Fusion Transition. *Traffic.* 14:650-662.

Karunakaran, S., T. Sasser, S. Rajalekshmi, and R. A. Fratti. 2012. SNAREs, HOPS, and regulatory lipids control the dynamics of vacuolar actin during homotypic fusion. *J Cell Sci.* 14:1683-1692.

Kilchert, C., and A. Spang. 2011. Cotranslational transport of ABP140 mRNA to the distal pole of S. cerevisiae. *EMBO J.* 30:3567-3580.

Klionsky, D. J., and S. D. Emr. 1989. Membrane protein sorting: biosynthesis, transport and processing of yeast vacuolar alkaline phosphatase. *EMBO J.* 8:2241-2250.

Klose, C., C. S. Ejsing, A. J. García-Sáez, H. J. Kaiser, J. L. Sampaio, M. A. Surma, A. Shevchenko, P. Schwille, and K. Simons. 2010. Yeast lipids can phase-separate into micrometer-scale membrane domains. *J Biol Chem.* 285:30224-30232.

Kohlwein, S. D., S. Eder, C. S. Oh, C. E. Martin, K. Gable, D. Bacikova, and T. Dunn. 2001. Tsc13p is required for fatty acid elongation and localizes to a novel structure at the nuclear-vacuolar interface in Saccharomyces cerevisiae. *Mol Cell Biol.* 21:109-125.

Krause, S. A., M. J. Cundell, P. P. Poon, J. McGhie, G. C. Johnston, C. Price, and J. V. Gray. 2012. Functional specialisation of yeast Rho1 GTP exchange factors. *J Cell Sci.* 125:2721-2731.

Kulakowski, G., H. Bousquet, J. B. Manneville, P. Bassereau, B. Goud, and L. K. Oesterlin. 2018. Lipid packing defects and membrane charge control RAB GTPase recruitment. *Traffic.* 19:536-545.

Kvam, E., K. Gable, T. M. Dunn, and D. S. Goldfarb. 2005. Targeting of Tsc13p to nucleus-vacuole junctions: a role for very-long-chain fatty acids in the biogenesis of microautophagic vesicles. *Mol Biol Cell.* 16:3987-3998.

Lachmann, J., F. A. Barr, and C. Ungermann. 2012. The Msb3/Gyp3 GAP controls the activity of the Rab GTPases Vps21 and Ypt7 at endosomes and vacuoles. *Mol Biol Cell.* 23:2516-2526.

Langemeyer, L., A. Perz, D. Kümmel, and C. Ungermann. 2018. A guanine nucleotide exchange factor (GEF) limits Rab GTPase-driven membrane fusion. *J Biol Chem.* 293:731-739.

Lester, R. L., G. B. Wells, G. Oxford, and R. C. Dickson. 1993. Mutant strains of Saccharomyces cerevisiae lacking sphingolipids synthesize novel inositol glycerophospholipids that mimic sphingolipid structures. *J Biol Chem.* 268:845-856.

Li, S. C., T. T. Diakov, T. Xu, M. Tarsio, W. Zhu, S. Couoh-Cardel, L. S. Weisman, and P. M. Kane. 2014. The signaling lipid $PI(3,5)P_2$ stabilizes V_1-V(o) sector interactions and activates the V-ATPase. *Mol Biol Cell.* 25:1251-1262.

Lockshon, D., C. P. Olsen, C. L. Brett, A. Chertov, A. J. Merz, D. A. Lorenz, M. R. Van Gilst, and B. K. Kennedy. 2012. Rho signaling participates in membrane fluidity homeostasis. *PLoS One.* 7:e45049.

Logan, M. R., L. Jones, and G. Eitzen. 2010. Cdc42p and Rho1p are sequentially activated and mechanistically linked to vacuole membrane fusion. *Biochem Biophys Res Commun.* 394:64-69.

Logan, M. R., L. Jones, D. Forsberg, A. Bodman, A. Baier, and G. Eitzen. 2011. Functional analysis of RhoGDI inhibitory activity on vacuole membrane fusion. *Biochem J.* 434:445-457.

Mattie, S., E. K. McNally, M. A. Karim, H. Vali, and C. L. Brett. 2017. How and why intralumenal membrane fragments form during vacuolar lysosome fusion. *Mol Biol Cell.* 28:309-321.

Mayer, A., and W. Wickner. 1997. Docking of yeast vacuoles is catalyzed by the Ras-like GTPase Ypt7p after symmetric priming by Sec18p (NSF). *J Cell Biol.* 136:307-17.

Mayer, A., W. Wickner, and A. Haas. 1996. Sec18p (NSF)-driven release of Sec17p (alpha-SNAP) can precede docking and fusion of yeast vacuoles. *Cell.* 85:83-94.

McNally, E. K., M. A. Karim, and C. L. Brett. 2017. Selective Lysosomal Transporter Degradation by Organelle Membrane Fusion. *Dev Cell.* 40:151-167.

Megyeri, M., H. Riezman, M. Schuldiner, and A. H. Futerman. 2016. Making Sense of the Yeast Sphingolipid Pathway. *J Mol Biol.* 428:4765-4775.

Michaelson, D., J. Silletti, G. Murphy, P. D'Eustachio, M. Rush, and M. R. Philips. 2001. Differential localization of Rho GTPases in live cells: regulation by hypervariable regions and RhoGDI binding. *J Cell Biol.* 152:111-126.

Miner, G. E., and R. Fratti. 2019. Real-Time Fluorescence Detection of Calcium Efflux During Vacuolar Membrane Fusion. *Methods Mol Biol.* 1860:323-331.

Miner, G. E., M. L. Starr, L. R. Hurst, and R. A. Fratti. 2017. Deleting the DAG kinase Dgk1 augments yeast vacuole fusion through increased Ypt7 activity and altered membrane fluidity. *Traffic.* 18:315-329.

Miner, G. E., M. L. Starr, L. R. Hurst, R. P. Sparks, M. Padolina, and R. A. Fratti. 2016. The Central Polybasic Region of the Soluble SNARE (Soluble N-Ethylmaleimide-sensitive Factor Attachment Protein Receptor) Vam7 Affects Binding to Phosphatidylinositol 3-Phosphate by the PX (Phox Homology) Domain. *J Biol Chem.* 291:17651-17663.

Miner, G. E., K. D. Sullivan, A. Guo, B. C. Jones, L. R. Hurst, E. C. Ellis, M. L. Starr, and R. A. Fratti. 2019. Phosphatidylinositol 3,5-Bisphosphate Regulates the Transition between trans-SNARE Complex Formation and Vacuole Membrane Fusion. *Mol Biol Cell.* 30:201-208.

Molino, D., E. Van der Giessen, L. Gissot, K. Hématy, J. Marion, J. Barthelemy, Y. Bellec, S. Vernhettes, B. Satiat-Jeunemaître, T. Galli, D. Tareste, and J. D. Faure. 2014. Inhibition of very long acyl chain sphingolipid synthesis modifies membrane dynamics during plant cytokinesis. *Biochim Biophys Acta.* 1842:1422-1430.

Müller, O., M. J. Bayer, C. Peters, J. S. Andersen, M. Mann, and A. Mayer. 2002. The Vtc proteins in vacuole fusion: coupling NSF activity to V(0) trans-complex formation. *EMBO J.* 21:259-269.

Müller, O., H. Neumann, M. J. Bayer, and A. Mayer. 2003. Role of the Vtc proteins in V-ATPase stability and membrane trafficking. *J Cell Sci.* 116:1107-1115.

Nagiec, M. M., J. A. Baltisberger, G. B. Wells, R. L. Lester, and R. C. Dickson. 1994. The LCB2 gene of Saccharomyces and the related LCB1 gene encode subunits of serine palmitoyltransferase, the initial enzyme in sphingolipid synthesis. *Proc Natl Acad Sci U S A.* 91:7899-7902.

Obara, K., R. Kojima, and A. Kihara. 2013. Effects on vesicular transport pathways at the late endosome in cells with limited very long-chain fatty acids. *J Lipid Res.* 54:831-842.

Oh, C. S., D. A. Toke, S. Mandala, and C. E. Martin. 1997. ELO2 and ELO3, homologues of the Saccharomyces cerevisiae ELO1 gene, function in fatty acid elongation and are required for sphingolipid formation. *J Biol Chem.* 272:17376-17384.

Ohya, Y., H. Qadota, Y. Anraku, J. R. Pringle, and D. Botstein. 1993. Suppression of yeast geranylgeranyl transferase I defect by alternative prenylation of two target GTPases, Rho1p and Cdc42p. *Mol Biol Cell.* 4:1017-1025.

Ozaki, K., K. Tanaka, H. Imamura, T. Hihara, T. Kameyama, H. Nonaka, H. Hirano, Y. Matsuura, and Y. Takai. 1996. Rom1p and Rom2p are GDP/GTP exchange proteins (GEPs) for the Rho1p small GTP binding protein in Saccharomyces cerevisiae. *Embo J.* 15:2196-207. abs.html.

Paumi, C. M., J. Menendez, A. Arnoldo, K. Engels, K. R. Iyer, S. Thaminy, O. Georgiev, Y. Barral, S. Michaelis, and I. Stagljar. 2007. Mapping protein-protein interactions for the yeast ABC transporter Ycf1p by integrated split-ubiquitin membrane yeast two-hybrid analysis. *Mol Cell.* 26:15-25.

Pechlivanis, M., and J. Kuhlmann. 2006. Hydrophobic modifications of Ras proteins by isoprenoid groups and fatty acids--More than just membrane anchoring. *Biochim Biophys Acta.* 1764:1914-1931.

Peng, Y., F. Tang, and L. S. Weisman. 2006. Palmitoylation plays a role in targeting Vac8p to specific membrane subdomains. *Traffic.* 7:1378-1387.

Peter Slotte, J. 2013. Molecular properties of various structurally defined sphingomyelins -- correlation of structure with function. *Prog Lipid Res.* 52:206-219.

Peters, C., M. J. Bayer, S. Buhler, J. S. Andersen, M. Mann, and A. Mayer. 2001. Trans-complex formation by proteolipid channels in the terminal phase of membrane fusion. *Nature.* 409:581-588.

Price, A., D. Seals, W. Wickner, and C. Ungermann. 2000. The docking stage of yeast vacuole fusion requires the transfer of proteins from a cis-SNARE complex to a Rab/Ypt protein. *J Cell Biol.* 148:1231-8.

Qiu, Q. S., and R. A. Fratti. 2010. The Na+/H+ exchanger Nhx1p regulates the initiation of Saccharomyces cerevisiae vacuole fusion. *J Cell Sci.* 123:3266-3275.

Raghupathy, R., A. A. Anilkumar, A. Polley, P. P. Singh, M. Yadav, C. Johnson, S. Suryawanshi, V. Saikam, S. D. Sawant, A. Panda, Z. Guo, R. A. Vishwakarma, M. Rao, and S. Mayor. 2015. Transbilayer lipid interactions mediate nanoclustering of lipid-anchored proteins. *Cell.* 161:581-594.

Raymond, C. K., I. Howald-Stevenson, C. A. Vater, and T. H. Stevens. 1992. Morphological classification of the yeast vacuolar protein sorting mutants: evidence for a prevacuolar compartment in class E vps mutants. *Mol Biol Cell.* 3:1389-1402.

Reese, C., F. Heise, and A. Mayer. 2005. Trans-SNARE pairing can precede a hemifusion intermediate in intracellular membrane fusion. *Nature.* 436:410-414.

Reese, C., and A. Mayer. 2005. Transition from hemifusion to pore opening is rate limiting for vacuole membrane fusion. *J Cell Biol.* 171:981-990.

Resh, M. D. 2016. Fatty acylation of proteins: The long and the short of it. *Prog Lipid Res.* 63:120-131.

Röper, K., D. Corbeil, and W. B. Huttner. 2000. Retention of prominin in microvilli reveals distinct cholesterol-based lipid micro-domains in the apical plasma membrane. *Nat Cell Biol.* 2:582-592.

Rössler, H., C. Rieck, T. Delong, U. Hoja, and E. Schweizer. 2003. Functional differentiation and selective inactivation of multiple Saccharomyces cerevisiae genes involved in very-long-chain fatty acid synthesis. *Mol Genet Genomics.* 269:290-298.

Sartorel, E., C. Ünlü, M. Jose, A. Massoni-Laporte, J. Meca, J. B. Sibarita, and D. McCusker. 2018. Phosphatidylserine and GTPase activation control Cdc42 nanoclustering to counter dissipative diffusion. *Mol Biol Cell.* 29:1299-1310.

Seals, D. F., G. Eitzen, N. Margolis, W. T. Wickner, and A. Price. 2000. A Ypt/Rab effector complex containing the Sec1 homolog Vps33p is required for homotypic vacuole fusion. *Proc Natl Acad Sci U S A.* 97:9402-7.

Sezgin, E., I. Levental, S. Mayor, and C. Eggeling. 2017. The mystery of membrane organization: composition, regulation and roles of lipid rafts. *Nat Rev Mol Cell Biol.* 18:361-374.

Sikorski, R. S., and P. Hieter. 1989. A system of shuttle vectors and yeast host strains designed for efficient manipulation of DNA in Saccharomyces cerevisiae. *Genetics.* 122:19-27.

Smith, J. A., A. E. Hall, and M. D. Rose. 2017. Membrane curvature directs the localization of Cdc42p to novel foci required for cell-cell fusion. *J Cell Biol.* 216:3971-3980.

Song, L. 2006. A soluble form of phosphatase in Saccharomyces cerevisiae capable of converting farnesyl diphosphate into E,E-farnesol. *Appl Biochem Biotechnol.* 128:149-158.

Starai, V. J., Y. Jun, and W. Wickner. 2007. Excess vacuolar SNAREs drive lysis and Rab bypass fusion. *Proc Natl Acad Sci U S A.* 104:13551-13558.

Starr, M. L., and R. A. Fratti. 2019. The Participation of Regulatory Lipids in Vacuole Homotypic Fusion. *Trends Biochem Sci.* 44:546-554.

Starr, M. L., L. R. Hurst, and R. A. Fratti. 2016. Phosphatidic acid sequesters Sec18p from cis-SNARE complexes to inhibit priming. *Traffic.* 17:1091-1109.

Stroupe, C., K. M. Collins, R. A. Fratti, and W. Wickner. 2006. Purification of active HOPS complex reveals its affinities for phosphoinositides and the SNARE Vam7p. *Embo J.* 25:1579-1589.

Takatori, S., T. Tatematsu, J. Cheng, J. Matsumoto, T. Akano, and T. Fujimoto. 2016. Phosphatidylinositol 3,5-Bisphosphate-Rich Membrane Domains in Endosomes and Lysosomes. *Traffic.* 17:154-167.

Tavolari, S., A. Munarini, G. Storci, S. Laufer, P. Chieco, and T. Guarnieri. 2012. The decrease of cell membrane fluidity by the non-steroidal anti-inflammatory drug Licofelone inhibits epidermal growth factor receptor signalling and triggers apoptosis in HCA-7 colon cancer cells. *Cancer Lett.* 321:187-194.

Tedrick, K., T. Trischuk, R. Lehner, and G. Eitzen. 2004. Enhanced membrane fusion in sterol-enriched vacuoles bypasses the Vrp1p requirement. *Mol Biol Cell.* 15:4609-4621.

Thomä, N. H., A. Niculae, R. S. Goody, and K. Alexandrov. 2001. Double prenylation by RabGGTase can proceed without dissociation of the mono-prenylated intermediate. *J Biol Chem.* 276:48631-48636.

Tomioku, K. N., M. Shigekuni, H. Hayashi, A. Yoshida, T. Futagami, H. Tamaki, K. Tanabe, and A. Fujita. 2018. Nanoscale domain formation of phosphatidylinositol 4-phosphate in the plasma and vacuolar membranes of living yeast cells. *Eur J Cell Biol.* 97:269-278.

Toulmay, A., and W. A. Prinz. 2013. Direct imaging reveals stable, micrometer-scale lipid domains that segregate proteins in live cells. *J Cell Biol.* 202:35-44.

Tripp, J. D., J. L. Lilley, W. N. Wood, and L. K. Lewis. 2013. Enhancement of plasmid DNA transformation efficiencies in early stationary-phase yeast cell cultures. *Yeast.* 30:191-200.

Vida, T. A., and S. D. Emr. 1995. A new vital stain for visualizing vacuolar membrane dynamics and endocytosis in yeast. *J Cell Biol.* 128:779-792.

Vollmer, P., E. Will, D. Scheglmann, M. Strom, and D. Gallwitz. 1999. Primary structure and biochemical characterization of yeast GTPase-activating proteins with substrate preference for the transport GTPase Ypt7p. *Eur J Biochem.* 260:284-290.

Voynova, N. S., C. Roubaty, H. M. Vazquez, S. K. Mallela, C. S. Ejsing, and A. Conzelmann. 2015. Saccharomyces cerevisiae Is Dependent on Vesicular Traffic between the Golgi Apparatus and the Vacuole When Inositolphosphorylceramide Synthase Aur1 Is Inactivated. *Eukaryot Cell.* 14:1203-1216.

Wang, L., E. S. Seeley, W. Wickner, and A. J. Merz. 2002. Vacuole Fusion at a Ring of Vertex Docking Sites Leaves Membrane Fragments within the Organelle. *Cell.* 108:357-69.

Weisman, L. S. 2003. Yeast vacuole inheritance and dynamics. *Annu Rev Genet.* 37:435-460.

Wichmann, H., L. Hengst, and D. Gallwitz. 1992. Endocytosis in yeast: evidence for the involvement of a small GTP-binding protein (Ypt7p). *Cell.* 71:1131-1142.

Wickner, W., and R. Schekman. 2008. Membrane fusion. *Nat Struct Mol Biol.* 15:658-664.

Wickner, W. 2010. Membrane Fusion: Five Lipids, Four SNAREs, Three Chaperones, Two Nucleotides, and a Rab, All Dancing in a Ring on Yeast Vacuoles. *Annu Rev Cell Dev Biol.* 26:115-136.

Wu, H., and P. Brennwald. 2010. The function of two Rho family GTPases is determined by distinct patterns of cell surface localization. *Mol Cell Biol.* 30:5207-5217.

Yoshida, S., S. Bartolini, and D. Pellman. 2009. Mechanisms for concentrating Rho1 during cytokinesis. *Genes Dev.* 23:810-823.

Table 1. Strains used in this study

Strain	***Genotype***	***Source***
BJ3505	*MATa pep4::HIS3 prb1-D1.6R his3-200 lys2-801 trp1D101 (gal3) ura3-52 gal2 can1*	(Jones et al., 1982)
DKY6281	*MATa pho8::TRP1 leu2-3 leu 2-112 ura3-52 his3-D200 trp1-D901 lys2-801 suc2-9*	(Haas et al., 1994)
RFY87	*MATa pho8::TRP1 leu2-3 leu 2-112 ura3-52 his3-D200 trp1-D901 lys2-801 suc2-9 elo3::hphMX6*	This study
RFY88	*MATa pep4::HIS3 prb1-D1.6R his3-200 lys2-801 trp1D101 (gal3) ura3-52 gal2 can1 elo3::hphMX6*	This study
RFY89	*MATa pep4::HIS3 prb1-D1.6R his3-200 lys2-801 trp1D101 (gal3) ura3-52 gal2 can1 pRS416DsR-Rho1*	This study
RFY90	*MATa pep4::HIS3 prb1-D1.6R his3-200 lys2-801 trp1D101 (gal3) ura3-52 gal2 can1 elo3::hphMX6 pRS416DsR-Rho1*	This study
GFP-Ypt7	*MATa pep4::HIS3 prb1-D1.6R his3-200 lys2-801 trp1D101 (gal3) ura3-52 gal2 can1 ypt7::URA3 pGFP-Ypt7*	(Wang et al., 2002)
RFY93	*MATa pep4::HIS3 prb1-D1.6R his3-200 lys2-801 trp1D101 (gal3) ura3-52 gal2 can1 ypt7::URA3 elo3::hphMX6 pGFP-Ypt7*	(Wang et al., 2002), This study
RFY94	*MATa pep4::HIS3 prb1-D1.6R his3-200 lys2-801 trp1D101 (gal3) ura3-52 gal2 can1 p414-ADH1-N17-2xmCherry*	(Kilchert and Spang, 2011), This study
RFY95	*MATa pep4::HIS3 prb1-D1.6R his3-200 lys2-801 trp1D101 (gal3) ura3-52 gal2 can1 elo3::hphMX6 p414-ADH1-N17-2xmCherry*	(Kilchert and Spang, 2011), This study
BY4742	*MATα HIS3D1 LEU2D0 MET15D0 URA3D0*	Open Biosystems
RFY96	*BY4742, MATα HIS3D1 LEU2D0 MET15D0 URA3D0 elo3::hphMX6*	This study

Table 2. Primers used in this study

Primer	Sequence (5' → 3')
elo3F	CGGCTTTTTTCCGTTTGTTTACGAAACATAAACAG-TCATCTGTTTAGCTTGCCTTGTCC
elo3R	TTTTTTCTTTTTCATTCGCTGTCAAAAATTCTCGCTTCCGACACTG-GATGGCGGCGTTA
TEF F	TCACCCGGGTACCGACATGGAGGCCCAGAATAC
TEF R	TTTACCCGGGGTTGTTTATGTTCGGATGTGATGTGAG
dsR F	ATTTAACCCGGGATGGACAACACCGAGGACGTCAT
dsR R	CTGATACTGTTACCAACTTGTTGTGACTGGGAGCCGGAG-TGGCGGGC
Rho1F	CCGAGGCCCGCCACTCCGGCTCCCAGTCACAACAAGTTGGTAACAG
Rho1R	GAGAGATCGAGCTCCTCCTATAACAAGACACACTT

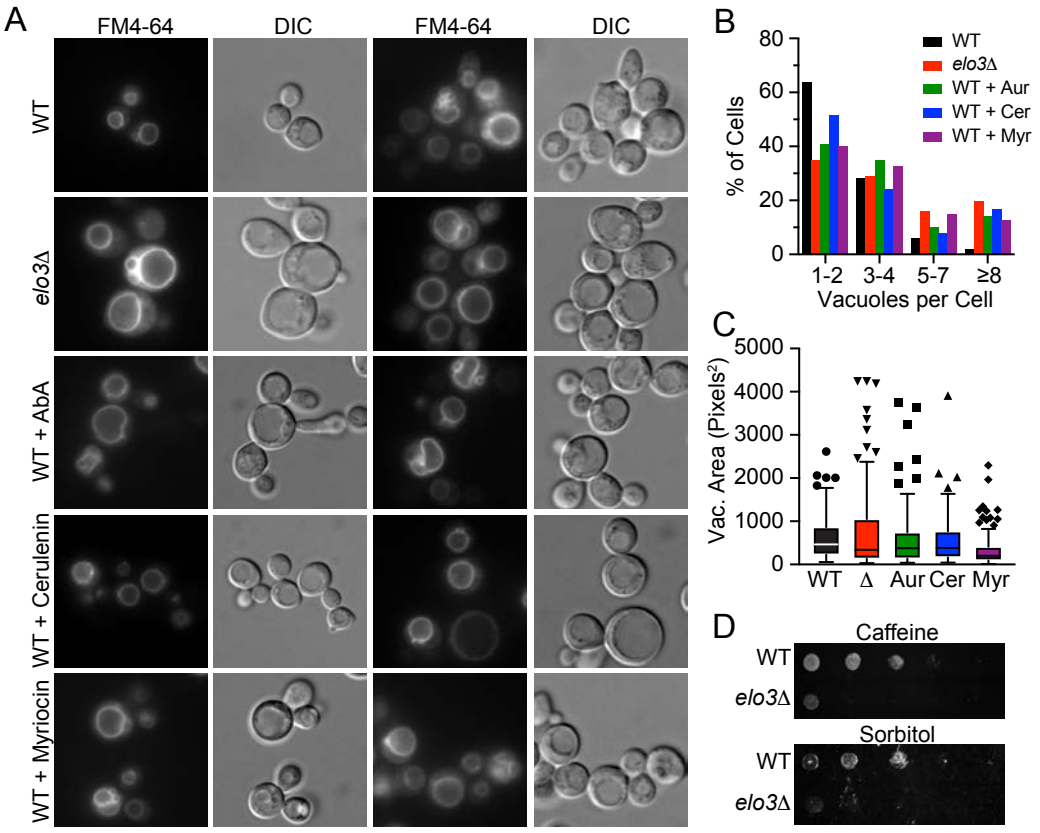

Figure 1. Vacuole morphology and is perturbed when sphingolipid synthesis is interrupted. (A) BJ3505 wild-type (WT) and *elo3*Δ yeast grown in YPD medium. Cells were grown overnight, back diluted to OD600 ~0.7 in fresh medium, and grown for an additional 2 hours. WT cells were then treated with aureobasidin A (0.125 µg/mL), myriocin (0.25 µg/mL), cerulenin (50 µM) or methanol (vehicle) and shaken for an additional 4-5 hours. Cells were then incubated with 10 µM MDY-64 for 15 minutes in the dark before visualization. Images are representative of multiple trials. (B) Inhibition of sphingolipid synthesis results in fragmented vacuolar phenotypes. Images of cells from (A) were used to count the number of vacuoles in each live yeast cell. Cells with more than 8 vacuoles were put in the same group (n = ~450 cells). (C) Inhibiting VLCFA and IPC synthesis results in large cells with Class F vacuole morphology. Using images from A the diameter of each vacuole compartment was calculated as the average length of two intersecting lines using ImageJ. Measurements were plotted as a box with a line representing the median area with upper and lower quartile values. The lines extending from each quartile box represent the minimum and maximum area in each dataset (n = ~140 cells). (D) Vacuole function is impaired in *elo3*Δ yeast. BJ3505 WT and *elo3*Δ yeast grown in YPD medium. Cells were grown overnight, back diluted to OD600 1.0 in fresh medium and serially diluted by a factor of 10. Three microliters of each dilution were spotted onto YPD agar plates containing either 6 mM caffeine or 1.8 M sorbitol. Plates were incubated at 30°C for 2-3 days before imaging. Images are representative of three trials.

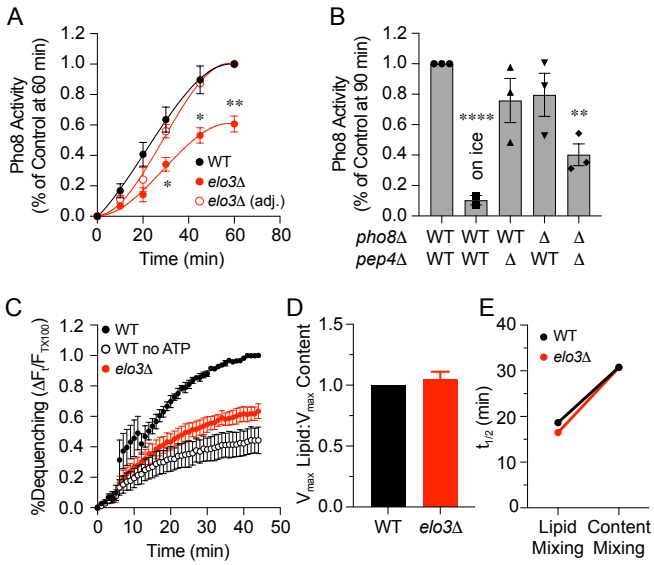

Figure 2. Elo3p enhances vacuole membrane fusion. (A) A time course of fusion activity was measured by mixing 3 µg of DKY6281 vacuoles and 3 µg of BJ3505 vacuoles then incubating samples at 27°C until the indicated time point, when the reactions were placed on ice. The red trace with open bubbles represents *elo3*Δ fusion when normalized to its own maximum, showing that the rate is decreased when cells lack VLCFAs. (B) Endpoint fusion reactions were performed with wild-type (WT) and *elo3*Δ vacuoles from the indicated strains in the bottom panel. DKY6281 yeast lack Pho8p and BJ3505 yeast lack Pep4p, and activation of proPho8p by Pep4p is only be achieved upon content mixing of vacuoles from different backgrounds. Fusion activity is expressed as the percentage of WT fusion activity by measuring the A400 of each sample after 90 min incubation at 27°C. (C) Elo3p enhances lipid mixing. Lipid mixing experiments were performed with vacuoles isolated from WT or *elo3*Δ BJ3505 yeast. Reporter vacuoles (2 µg) labeled with Rh-PE were incubated with 16 µg unlabeled vacuoles. Fluorescence (λ_{ex}=544nm, λ_{em}=590nm) was measured every 60s for 40 min following the addition of ATP (at t = 5 min). Error bars represent standard error of the mean (n = 3). (D) The lipid-to-content mixing ratio was calculated using the data in (A) and (B). (E) The times at half maximal lipid mixing, and content mixing for WT (black trace) and *elo3*Δ (red trace) vacuoles using data from (A) and (B). Error bars represent standard error of the mean (n = 3). **** p<0.0001, ** p<0.01, * p<0.05 (unpaired t test)

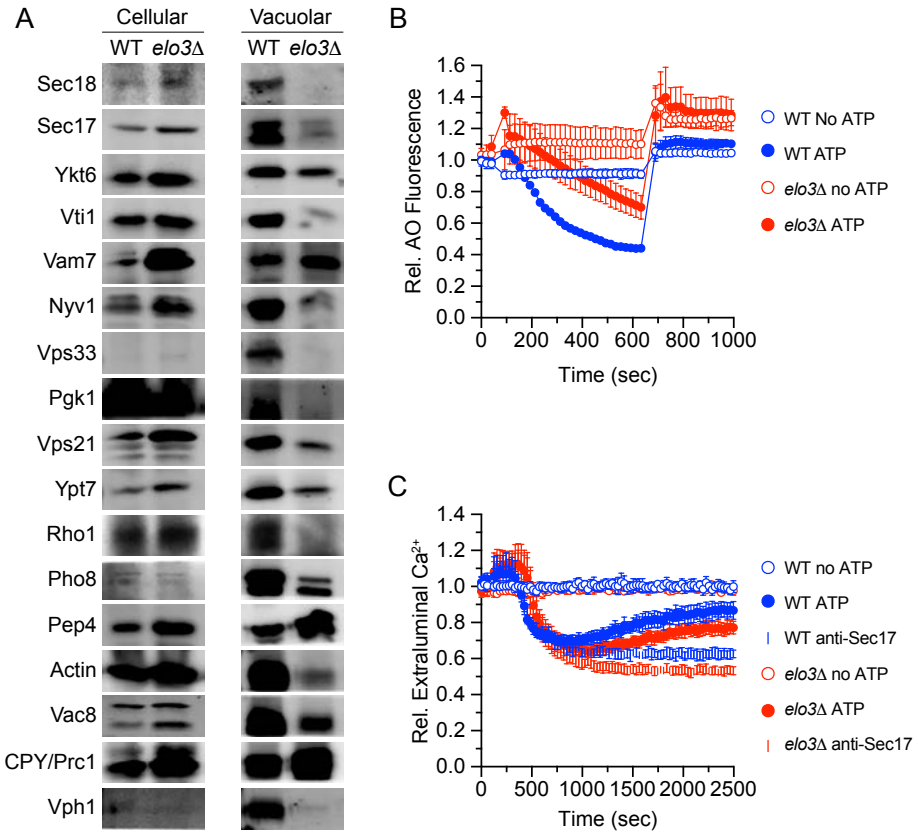

Figure 3. Trafficking of vacuolar fusion proteins is disrupted when cells lack Elo3p. (A) The presence of vacuole marker proteins was examined in total cell extracts (corresponding to 0.11OD_{600} units of cells) and isolated vacuoles (corresponding to 1 µg of protein determined by Bradford assay) by Western blot with antibodies raised against the indicated protein. Vacuoles isolated from the *elo3*Δ yeast have noticeably reduced amounts of vacuolar fusion proteins, except for Vam7p, Pep4p (PrA), and Prc1 (CPY). Experiments were performed with BY4742 yeast with the *ELO3* gene knocked via homologous recombination, which allowed Pep4p, and Pho8p levels to be analyzed simultaneously. (B) Proton pumping is reduced in vacuoles from *elo3*Δ yeast. Acridine orange fluorescence quenching was used to measure the proton pumping ability of vacuoles from WT and *elo3*Δ yeast. Control reactions consisting of vacuoles incubated without ATP or in the presence of 50 µM Bafilomycin A1 were included to specifically inhibit V-ATPase activity. Error bars represent standard error of the mean (n = 3). (C) Fusion reactions containing vacuoles isolated from WT or *elo3*Δ yeast incubated with 150 nM Cal-520 in the presence or absence of ATP regenerating system. Control reactions were inhibited by addition of 80 µg/mL of anti-Sec17 IgG to block priming and release of cis-SNARE bundles, which prevents the formation of any new trans-SNARE bundles and calcium efflux. Fluorescence signal was normalized to the control reaction without ATP. Error bars represent standard error of the mean (n = 3).

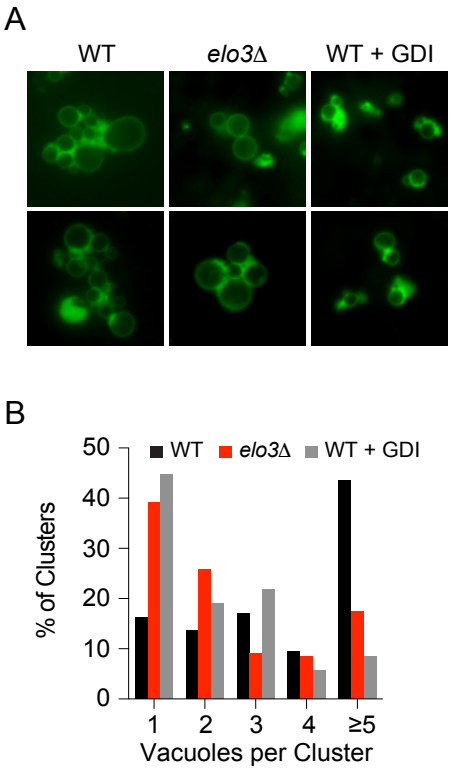

Figure 4. The docking sub-reaction is inhibited by a lack of C26 VLCFAs. Vacuoles were isolated as described and incubated for 20 minutes at 27°C under docking conditions. Following incubation reaction mixtures were placed on ice and gently mixed in the presence of the yeast vacuole marker MDY64. Wild-type vacuoles were incubated with purified 200 µg/mL GDI (Gdi1p) to specifically inhibit the Ypt7p-dependent tethering and subsequent docking of vacuoles. B. Quantification of the clustering of docked vacuoles from experiments in A. Approximately 300 vacuole clusters were counted for each condition.

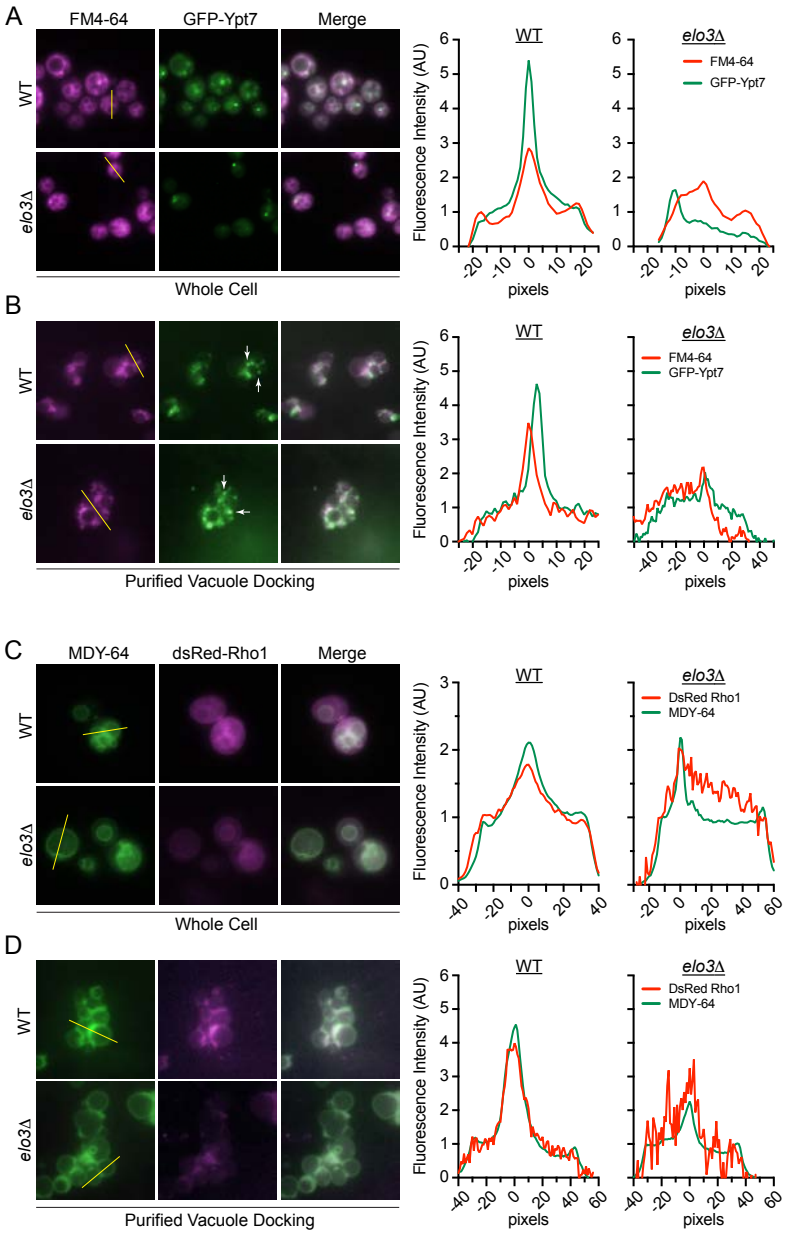

Figure 5. Small GTPases that regulate fusion are mislocalized in *elo3*Δ yeast. (A) Wild-type and *elo3*Δ yeast expressing GFP-Ypt7p were grown overnight in TRP- dropout media, back-diluted to 0.5 OD_{600} into fresh YPD, and allowed to grow for another ~5 hrs. Representative images of docked vacuoles with a line were used for the line scan analyses right of the micrographs. The red trace follows FM4-64 and the green trace follows GFP-Ypt7p fluorescence distributions (B). Micrographs showing docking reactions of WT and *elo3*Δ vacuoles from strains in (A). Arrows point to puncta that represent vertex domains of apposed vacuoles. (C) Wild-type and *elo3*Δ yeast expressing DsRed-Rho1p were grown overnight in URA- dropout

media, back diluted to 0.5 OD_{600} into fresh YPD, and allowed to grow for another ~5 hrs. Representative images of docked vacuoles with a line were used for the line scan analyses right of the micrographs. The green trace follows MDY64 and the red trace follows DsRed-Rho1 fluorescence distributions. (D) Micrographs of docking reactions of WT and *elo3*Δ vacuoles from strains in (C).

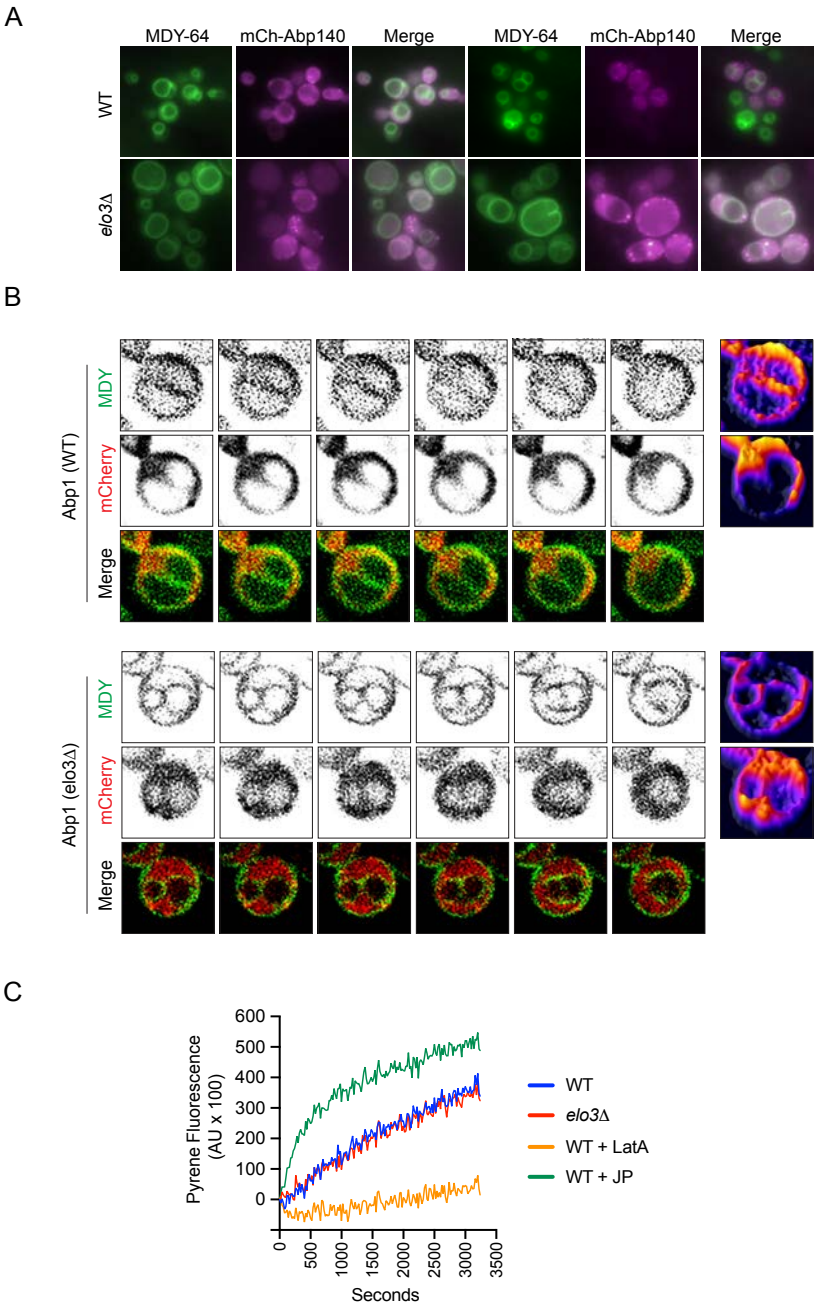

Figure 6. C26 VLCFAs influence actin localization, but not the vacuole's ability to stimulate actin polymerization. (A) Live microscopy of BJ3505 wild-type and *elo3*Δ yeast expressing the p414-ADH1-N17-2xmCherry plasmid. MDY-64 was used to visualize the vacuole membrane. (B) Micrographs of live yeast cells expressing the Abp140 construct undergoing a fusion cycle *in vivo*. The far-right panels show the MDY64 (top) and mCherry (bottom) fluorescence intensity profile plots. The mCherry signal is much more intense in the cytoplasm and the boundary domain between vacuoles. (C) *in vitro* actin polymerization

assay. Vacuoles were isolated from BJ3505 wild-type and *elo3*Δ yeast. Vacuoles were preincubated in fusion reaction buffer for 30 minutes before the addition of pyrene muscle actin. Wild-type vacuoles were also incubated in the presence of 10 μM jasplakinolide (to stimulate polymerization) or 10 μM latrunculin A (to inhibit polymerization).

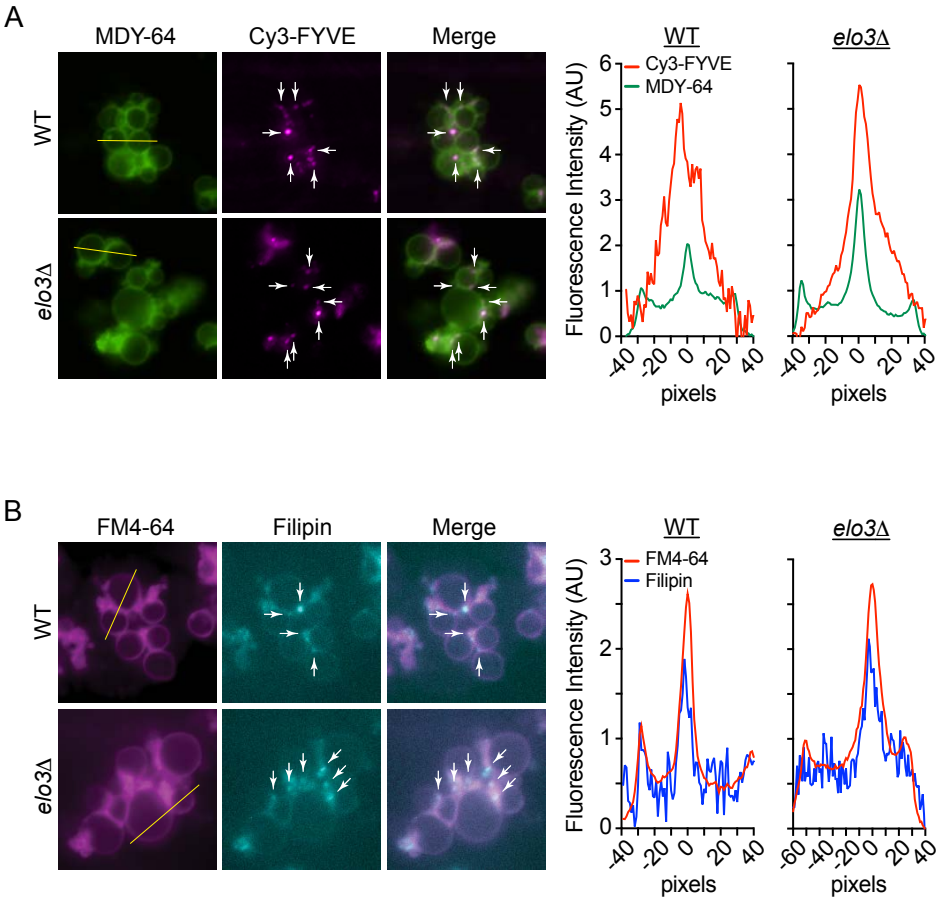

Figure 7. Regulatory lipids which enrich at the vertex are largely unaffected by the loss of Elo3p. (A) Docking reactions containing 6 µg of purified vacuoles were performed in the presence of 0.25 µM Cy3-FYVE. Yeast Vacuole Marker MDY-64 was added at the end of the reaction and docked vacuoles were visualized under the microscope. Arrows point to signal enrichment at the vertices of docked vacuoles. Line scan analyses were performed in ImageJ to measure the distribution of fluorescent signal. (B) Docking reactions performed in the presence of 5 µM filipin III. FM4-64 was added at the end of the reaction and docked vacuoles were visualized under the microscope. Arrows point to signal enrichment at the vertices of docked vacuoles. Line scan analyses were performed in ImageJ to measure the distribution of fluorescent signal.

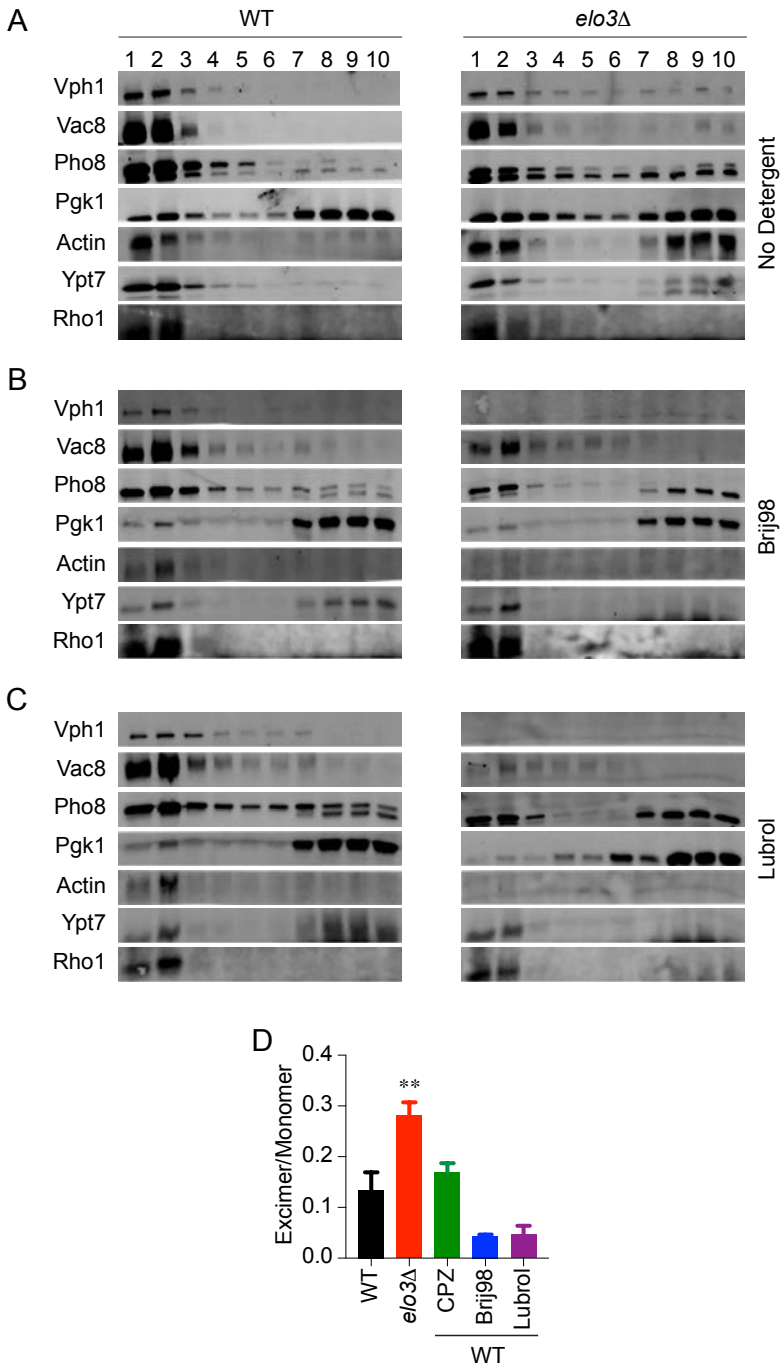

Figure 8. Fusion proteins are solubilized from vacuole membrane nanodomains when yeast lack VLCFAs. Vacuoles isolated from wild-type and *elo3*Δ BY4742 yeast were incubated in the absence (A) or presence of [0.5% (w/v) Brij98 (B) or 0.5% (w/v) Lubrol WX (C)] at 4°C and separated through a 0-40% (w/v) Optiprep floatation gradient. Samples collected from the top (fraction 1) to the bottom (fraction 10) of the gradient and subjected to SDS-PAGE and immunoblot analyses for the indicated fusion proteins. (D)

Vacuoles isolated from the *elo3*Δ yeast are more fluid than wild-type vacuoles. Isolated vacuoles (50 µL of 0.5 mg/mL vacuole isolation) were mixed with 50 µL of 20 µM PDA in PS+pluronic F127. After incubation in the dark for 20 minutes at room temperature, the fluorescence of PDA species (monomer/excimer) was measured (λ_{ex} = 355 nm, λ_{em}(monomer) = 410 nm, λ_{em}(excimer) = 520 nm). The membrane fluidity is then represented as the ration of excimer/monomer fluorescence. Chlorpromazine (CPZ, 10 µM) was included to artificially increase the fluidity of vacuoles isolated from wild type yeast. Error bars represent SEM (n=3). ** $p<0.01$ (unpaired t test).